
Learning to Integrate Diffusion ODEs by Averaging the Derivatives

Wenze Liu Xiangyu Yue*

MMLab, The Chinese University of Hong Kong

Abstract

To accelerate diffusion model inference, numerical solvers perform poorly at extremely small steps, while distillation techniques often introduce complexity and instability. This work presents an intermediate strategy, balancing performance and cost, by learning ODE integration using loss functions derived from the derivative-integral relationship, inspired by Monte Carlo integration and Picard iteration. From a geometric perspective, the losses operate by gradually extending the tangent to the secant, thus are named as secant losses. The target of secant losses is the same as that of diffusion models, or the diffusion model itself, leading to great training stability. By fine-tuning or distillation, the secant version of EDM achieves a 10-step FID of 2.14 on CIFAR-10, while the secant version of SiT-XL/2 attains a 4-step FID of 2.27 and an 8-step FID of 1.96 on ImageNet-256 \times 256. Code is available at <https://github.com/poppuppy/secant-expectation>.

1 Introduction

Diffusion models [1, 2, 3, 4] generate images by reversely denoising their noised versions, which can be formulated by stochastic differential equations (SDEs) and the corresponding probability flow ordinary differential equations (PF-ODEs) [4]. Over recent years, diffusion models have transformed the landscape of generative modeling, across multiple modalities such as image [5, 6, 7, 8], video [9, 10, 11] and audio [12, 13, 14]. Despite their remarkable performance, a significant drawback of diffusion models is their slow inference speed: they typically require hundreds to thousands of number of function evaluations (NFEs) to generate a single image. Considerable research has focused on reducing the number of required steps, with common approaches falling into categories including faster samplers [15, 16, 17, 18] for diffusion SDEs or PF-ODEs, and diffusion distillation [19, 20, 21, 22, 23, 24, 25, 26, 27, 28, 29, 30, 31, 32, 33, 34, 35] methods that distill pretrained diffusion models to few-step generators. However, faster samplers experience significant performance degradation when operating with a small number of function evaluations (typically fewer than 10 NFEs). Meanwhile, distillation approaches frequently introduce substantial computational overhead, complex training procedures, or training instabilities. Additionally, they sometimes face risks of model collapse and over-smoothing in the generated outputs.

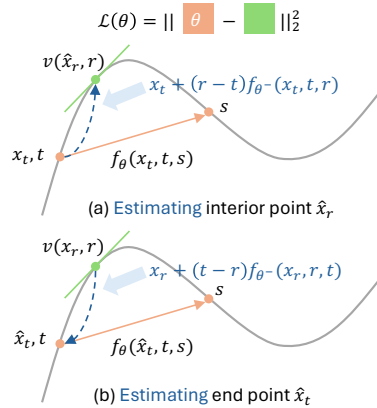


Figure 1: Formulation of secant losses. We employ an ℓ_2 loss between the learned secant and a tangent at a random interior time point. By estimating either the interior or the end point, we derive two variants shown in (a) and (b).

*Corresponding author.



Figure 2: Selected 8-step samples on ImageNet 256×256 .

In this work, we propose a simple intermediate solution to reduce the inference steps of diffusion models through easy distillation or fine-tuning. A diffusion model constructs the PF-ODE by fitting the derivative of the noised image with respect to time, as indicated by the green line in Fig. 1. From a geometric perspective, we refer to the diffusion model as the *tangent* since it describes the instantaneous rate of change of the noised image as the time difference approaches zero. Correspondingly, we define the rate of change of the noised image between two time points as the *secant*, marked in orange in the figure. Unlike diffusion models, we use neural networks to model the secant function instead. Based on the observation that the secant is the average of all tangents between two time points, we establish an integral equation as our loss function, termed *secant losses*. This average is implemented by taking the expectation with respect to random time variables in a Monte Carlo fashion. Since we can only sample one noised image for evaluating either the secant or the tangent at each training iteration, we let the model estimate the other, inspired by Picard iteration. Two scenarios for estimating the interior or the end point are shown in Fig. 1 (a) and (b), respectively. This results in a straightforward loss formulation: the distance between the learned secant with respect to two given time points and a tangent at a random intermediate time between them, as presented at the top of Fig. 1. Intuitively, secant losses work by gradually extending from the tangent to the secant. Unlike consistency models [33, 35, 34, 36], which either introduce discretization errors or rely on explicit differentiation in loss calculation, our approach avoids explicit differentiation while preserving accurate solutions at sufficiently small time intervals under mild conditions. More importantly, the target of our secant losses is identical to that of diffusion models or the diffusion model itself. This parallel to diffusion models provides significantly greater training stability compared with consistency models.

We evaluate our method on CIFAR-10 [37] and ImageNet- 256×256 [38] datasets, using EDM [6] and SiT [39] as teacher diffusion models, respectively. Our experiments demonstrate that diffusion models can be efficiently converted to their secant version, with significantly slower accuracy degradation compared to conventional numerical solvers as the step number decreases. On CIFAR-10, our approach achieves FID scores of 2.14 with 10 steps. For ImageNet- 256×256 in latent space, we obtain a 4-step FID of 2.78 and an 8-step FID of 2.33. With the guidance interval technique [40], the performance is further improved to 2.27 with 4 steps and 1.96 with 8 steps.

2 Related Work

Few-step diffusion distillation and training. Reducing inference steps in diffusion models is commonly achieved through distillation. As an application of knowledge distillation [41], direct distillation methods [19, 20] generate noise-image pairs by sampling from a pretrained diffusion model and train a one-step model on this synthetic dataset. Similarly, progressive distillation [21, 22] iteratively trains the models to merge adjacent steps toward a one-step model. These methods often introduce significant computational overhead due to extensive sampling or training costs. Adversarial distillation approaches [23, 24, 25] apply GAN-style losses [42] to supervise the one-step distribution,

potentially increasing training instability. Variational score distillation [26, 27, 28, 29, 30, 31, 32] and score identity distillation [43, 44] also employ distribution-level distillation, while introduce additional complexity due to the simultaneous optimization of two online models, and may potentially result in over-smoothing artifacts in the generated outputs. Consistency distillation [33, 34, 35] leverages the consistency property of PF-ODEs to train models to solve these equations directly, but faces stability challenges [33, 35] and may require model customization [35]. While direct training of consistency models [33, 45, 35] is feasible, they typically underperform consistency distillation under high data variance [35]. Similarly, Shortcut Models [46] utilize the consistency property as regularization in the loss function, which could be considered as simultaneously training and distillation. Rectified flow [47, 48] adopts a multi-time training strategy aimed at gradually straightening the trajectory of the PF-ODE. Similar to consistency models, our work also introduces losses for both distillation and training. However, our loss function emphasizes local accuracy, which enhances stability, though the accuracy decreases more at larger time intervals.

Fast diffusion samplers. Common numerical solvers, such as the Euler solver for PF-ODEs and the Euler-Maruyama solver for SDEs, typically require hundreds to thousands of NFEs to sample an image from diffusion models. Since SDEs involve greater randomness, samplers based on them generally require much more NFEs to converge [2, 49, 4, 6, 50, 51, 52, 53]. Consequently, existing fast samplers are usually based on PF-ODEs, including both training-free and learnable methods. Training-free methods leverage mathematical tools to analyze and formulate the solving process. Examples include high-order samplers like the Heun sampler [6], exponential samplers [15, 16, 17, 54, 55], and parallel samplers [56, 57]. Despite their convenience, these methods struggle in low NFE scenarios. Data-driven, learnable samplers enhance performance by training lightweight modules to learn hyperparameters in the sampling process, such as coefficients [58], high-order derivatives [59], and time schedules [18, 60, 61, 62, 63, 64]. However, both training-free and learned faster samplers still experience significant performance degradation when the step count falls below ten. Our method is also based on solving the diffusion ODE, and it degrades more gradually than conventional diffusion samplers as the step count decreases. Our approach can be seen as an effective compromise between fast samplers and diffusion distillation methods.

3 Diffusion Models

For simplicity, we review diffusion models within the flow matching framework [65, 47, 66]. Let p_d denote the data distribution, and $\mathbf{x}_0 \sim p_d$ represent a data sample. Let $\mathbf{z} \sim \mathcal{N}(\mathbf{0}, \mathbf{I})$ be a standard Gaussian sample. The noised image with respect to \mathbf{x}_0 and \mathbf{z} at time t is defined as $\mathbf{x}_t = \alpha_t \mathbf{x}_0 + \sigma_t \mathbf{z}$, where $t \in [0, 1]$ represents the intensity of added noise. For a given neural network \mathbf{v}_θ , the training objective is formulated as:

$$\mathcal{L}_{\text{Diff}}(\theta) = \mathbb{E}_{\mathbf{x}_0, \mathbf{z}, t} \|\mathbf{v}_\theta(\mathbf{x}_t, t) - (\alpha'_t \mathbf{x}_0 + \sigma'_t \mathbf{z})\|_2^2, \quad (1)$$

where α'_t and σ'_t are time derivatives. An established result from the literature on diffusion and flow matching [65, 47, 66] is as follows:

Proposition 1. *When $\mathcal{L}_{\text{Diff}}(\theta)$ reaches the minimum, the optimal solution $\mathbf{v}_\theta^*(\mathbf{x}_t, t)$ is*

$$\mathbf{v}(\mathbf{x}_t, t) = \mathbb{E}_{\mathbf{x}_0, \mathbf{z}} (\alpha'_t \mathbf{x}_0 + \sigma'_t \mathbf{z} | \mathbf{x}_t). \quad (2)$$

And the associated PF-ODE

$$\frac{d\mathbf{x}_t}{dt} = \mathbf{v}(\mathbf{x}_t, t) \quad (3)$$

is guaranteed to generate $\mathbf{x}_0 \sim p_d$ at $t = 0$ starting from $\mathbf{z} \sim \mathcal{N}(\mathbf{0}, \mathbf{I})$ at $t = 1$.

4 Learning Integral with Secant Expectation

In this section, we first introduce how to parametrize the model as the secant function. We then explain our derivation of loss functions based on Monte Carlo integration and Picard iteration.

4.1 Secant Parametrization

Given the PF-ODE Eq. (3), to solve \mathbf{x}_s at time s starting from \mathbf{x}_t at time t , one calculates

$$\mathbf{x}_s = \mathbf{x}_t + \int_t^s \mathbf{v}(\mathbf{x}_r, r) dr. \quad (4)$$

Algorithm 1 Secant Distillation by Estimating the Interior Point (SDEI)

Input: dataset \mathcal{D} , neural network \mathbf{f}_θ , teacher diffusion model \mathbf{v} , learning rate η

repeat

- $\theta^- \leftarrow \theta$
- Sample $\mathbf{x} \sim \mathcal{D}$, $\mathbf{z} \sim \mathcal{N}(\mathbf{0}, \mathbf{I})$
- Sample t and s
- Sample $r \sim \mathcal{U}[0, 1]$, $r \leftarrow t + r(s - t)$
- $\mathbf{x}_t \leftarrow t\mathbf{x} + (1 - t)\mathbf{z}$
- $\hat{\mathbf{x}}_r \leftarrow \mathbf{x}_t + (r - t)\mathbf{f}_{\theta^-}(\mathbf{x}_t, t, r)$
- $\mathbf{v}_r \leftarrow \mathbf{v}(\hat{\mathbf{x}}_r, r)$
- $\mathcal{L}(\theta) = \mathbb{E}_{\mathbf{x}, \mathbf{z}, t, s, r} \|\mathbf{f}_\theta(\mathbf{x}_t, t, s) - \mathbf{v}_r\|_2^2$
- $\theta \leftarrow \theta - \eta \nabla_\theta \mathcal{L}(\theta)$

until convergence

Algorithm 2 Secant Training by Estimating the End Point (STEE)

Input: dataset \mathcal{D} , neural network \mathbf{f}_θ , learning rate η

repeat

- $\theta^- \leftarrow \theta$
- Sample $\mathbf{x} \sim \mathcal{D}$, $\mathbf{z} \sim \mathcal{N}(\mathbf{0}, \mathbf{I})$
- Sample t and s
- Sample $r \sim \mathcal{U}[0, 1]$, $r \leftarrow t + r(s - t)$
- $\mathbf{x}_r \leftarrow r\mathbf{x} + (1 - r)\mathbf{z}$
- $\hat{\mathbf{x}}_t \leftarrow \mathbf{x}_r + (t - r)\mathbf{f}_{\theta^-}(\mathbf{x}_r, r, t)$
- $\mathbf{u}_r \leftarrow \mathbf{x} - \mathbf{z}$
- $\mathcal{L}(\theta) = \mathbb{E}_{\mathbf{x}, \mathbf{z}, t, s, r} \|\mathbf{f}_\theta(\hat{\mathbf{x}}_t, t, s) - \mathbf{u}_r\|_2^2$
- $\theta \leftarrow \theta - \eta \nabla_\theta \mathcal{L}(\theta)$

until convergence

We define the secant function from \mathbf{x}_t at time t to time s as

$$\mathbf{f}(\mathbf{x}_t, t, s) = \begin{cases} \mathbf{v}(\mathbf{x}_t, t), & \text{if } t = s, \\ \frac{1}{s - t} \int_t^s \mathbf{v}(\mathbf{x}_r, r) dr, & \text{if } t \neq s. \end{cases} \quad (5)$$

Since

$$\mathbf{f}(\mathbf{x}_t, t, t) = \lim_{s \rightarrow t} \mathbf{f}(\mathbf{x}_t, t, s) = \lim_{s \rightarrow t} \frac{1}{s - t} \int_t^s \mathbf{v}(\mathbf{x}_r, r) dr = \mathbf{v}(\mathbf{x}_t, t), \quad (6)$$

$\mathbf{f}(\mathbf{x}_t, t, s)$ is continuous at $s = t$. And, we parametrize the neural network $\mathbf{f}_\theta(\mathbf{x}_t, t, s)$ to represent this secant function. If $\mathbf{f}_\theta(\mathbf{x}_t, t, s)$ is trained accurately fitting $\mathbf{f}(\mathbf{x}_t, t, s)$, we can directly jump from \mathbf{x}_t to \mathbf{x}_s using

$$\mathbf{x}_s = \mathbf{x}_t + \int_t^s \mathbf{v}(\mathbf{x}_r, r) dr = \mathbf{x}_t + (s - t)\mathbf{f}_\theta(\mathbf{x}_t, t, s). \quad (7)$$

We choose this parameterization for its simplicity and clearer geometric interpretation, though other similar formulations [34, 36, 46] would also be viable in practice.

4.2 Secant Expectation

Examining Eq. (5) from a probabilistic perspective, we have

$$\mathbf{f}(\mathbf{x}_t, t, s) = \frac{1}{s - t} \int_t^s \mathbf{v}(\mathbf{x}_r, r) dr = \mathbb{E}_{r \sim U(t, s)} \mathbf{v}(\mathbf{x}_r, r), \quad (8)$$

which indicates that we can calculate the integral $\frac{1}{s - t} \int_t^s \mathbf{v}(\mathbf{x}_r, r) dr$ by uniformly sampling random values of $r \sim \mathcal{U}(t, s)$ ² and computing their average. However, during training, we cannot obtain a large number of \mathbf{x}_r 's to calculate this integral accurately. We address this challenge by formulating the integral as the optimal solution to a simple objective that involves only one \mathbf{x}_r at a time:

$$\mathcal{L}_{\text{Naïve}}(\theta) = \mathbb{E}_{\mathbf{x}_0, \mathbf{z}, r \sim U(t, s)} \|\mathbf{f}_\theta(\mathbf{x}_t, t, s) - \mathbf{v}(\mathbf{x}_r, r)\|_2^2. \quad (9)$$

This approach is inspired by the diffusion objective that leads from Eq. (1) to Eq. (2). Inspecting Eq. (9), we observe that we can only access either \mathbf{x}_t or \mathbf{x}_r at each training step, but not both simultaneously. To address this issue, we draw inspiration from Picard iteration by estimating one of the solutions between \mathbf{x}_t and \mathbf{x}_r given the other. We refer to the family of obtained loss functions in this way as *secant losses*. Specifically, one way is to sample $\mathbf{x}_t = \alpha_t \mathbf{x}_0 + \sigma_t \mathbf{z}$, and estimate \mathbf{x}_r using

$$\hat{\mathbf{x}}_r = \mathbf{x}_t + (r - t)\mathbf{f}_{\theta^-}(\mathbf{x}_t, t, r), \quad (10)$$

²We do not assume specific order relation between t and s , and we slightly abuse the notion $r \sim \mathcal{U}(t, s)$ by meaning $r \sim \mathcal{U}(\min\{t, s\}, \max\{t, s\})$ for simplicity.

where θ^- denotes the `stop_gradient` version of θ . This transforms the loss function in Eq. (9) into

$$\mathcal{L}_{\text{SDEI}}(\theta) = \mathbb{E}_{\mathbf{x}_0, \mathbf{z}, t, s, r \sim \mathcal{U}(t, s)} \|\mathbf{f}_\theta(\mathbf{x}_t, t, s) - \mathbf{v}(\mathbf{x}_t + (r - t)\mathbf{f}_{\theta^-}(\mathbf{x}_t, t, r), r)\|_2^2, \quad (11)$$

where $\mathcal{L}_{\text{SDEI}}$ stands for *secant distillation by estimating the interior point*, meaning we sample at the end point t and estimate the interior solution at r . According to Eq. (6), we can also directly train the few-step model by incorporating the diffusion loss termed as

$$\begin{aligned} \mathcal{L}_{\text{STEI}}(\theta) = \mathbb{E}_{\mathbf{x}_0, \mathbf{z}, t, s, r \sim \mathcal{U}(t, s)} & \|\mathbf{f}_\theta(\mathbf{x}_t, t, s) - \mathbf{f}_{\theta^-}(\mathbf{x}_t + (r - t)\mathbf{f}_{\theta^-}(\mathbf{x}_t, t, r), r, r)\|_2^2 \\ & + \lambda \mathbb{E}_{\mathbf{x}_0, \mathbf{z}, \tau} \|\mathbf{f}_\theta(\mathbf{x}_\tau, \tau, \tau) - (\alpha'_\tau \mathbf{x}_0 + \sigma'_\tau \mathbf{z})\|_2^2, \end{aligned} \quad (12)$$

where λ is a constant to balance diffusion loss and secant loss, and τ is a time step indicating the time sampling in the two parts is independent. Here STEI denotes *secant training by estimating the interior point*.

Alternatively, we can sample $\mathbf{x}_r = \alpha_r \mathbf{x}_0 + \sigma_r \mathbf{z}$ and estimate the solution at t from r as

$$\hat{\mathbf{x}}_t = \mathbf{x}_r + (t - r)\mathbf{f}_{\theta^-}(\mathbf{x}_r, r, t), \quad (13)$$

which we term *secant distillation by estimating the end point (SDEE)*. The loss from Eq. (9) then becomes

$$\mathcal{L}_{\text{SDEE}}(\theta) = \mathbb{E}_{\mathbf{x}_0, \mathbf{z}, t, s, r \sim \mathcal{U}(t, s)} \|\mathbf{f}_\theta(\mathbf{x}_r + (t - r)\mathbf{f}_{\theta^-}(\mathbf{x}_r, r, t), t, s) - \mathbf{v}(\mathbf{x}_r, r)\|_2^2. \quad (14)$$

In the above equation, since we directly use the sampled \mathbf{x}_r to evaluate $\mathbf{v}(\mathbf{x}_r, r)$, we can alternatively use $\alpha'_r \mathbf{x}_0 + \sigma'_r \mathbf{z}$ to estimate $\mathbf{v}(\mathbf{x}_r, r)$ like diffusion models do in Eq. (1) to Eq. (2). This leads to the training version termed as *secant training by estimating the end point (STEE)*:

$$\mathcal{L}_{\text{STEE}}(\theta) = \mathbb{E}_{\mathbf{x}_0, \mathbf{z}, t, s, r \sim \mathcal{U}(t, s)} \|\mathbf{f}_\theta(\mathbf{x}_r + (t - r)\mathbf{f}_{\theta^-}(\mathbf{x}_r, r, t), t, s) - (\alpha'_r \mathbf{x}_0 + \sigma'_r \mathbf{z})\|_2^2. \quad (15)$$

As theoretical justification for the above losses, we present the following theorems, which corresponds to $\mathcal{L}_{\text{SDEI}}(\theta)$ and $\mathcal{L}_{\text{STEE}}(\theta)$. The other two can be derived from these.

Theorem 2 (SDEI). *Let $\mathbf{f}_\theta(\mathbf{x}_t, t, s)$ be a neural network, and $\mathbf{v}(\mathbf{x}_t, t) = \mathbb{E}(\alpha'_t \mathbf{x}_0 + \sigma'_t \mathbf{z} | \mathbf{x}_t)$. Assume $\mathbf{v}(\mathbf{x}_t, t)$ is L -Lipschitz continuous in its first argument, i.e., $\|\mathbf{v}(\mathbf{x}_1, t) - \mathbf{v}(\mathbf{x}_2, t)\|_2 \leq L \|\mathbf{x}_1 - \mathbf{x}_2\|_2$ for all $\mathbf{x}_1, \mathbf{x}_2 \in \mathbb{R}^n$, $t \in [0, 1]$. Then, for each fixed t , in a sufficient small neighborhood $|s - t| \leq h$ for some $h > 0$, if $\mathcal{L}_{\text{SDEI}}(\theta)$ reaches its minimum, we have $\mathbf{f}_\theta(\mathbf{x}_t, t, s) = \mathbf{f}(\mathbf{x}_t, t, s)$.*

Theorem 3 (STEE). *Let $\mathbf{f}_\theta(\mathbf{x}_t, t, s)$ be a neural network, and $\mathbf{v}(\mathbf{x}_t, t) = \mathbb{E}(\alpha'_t \mathbf{x}_0 + \sigma'_t \mathbf{z} | \mathbf{x}_t)$. Assume $\mathbf{f}_\theta(\mathbf{x}_t, t, s)$ is L -Lipschitz continuous in its first argument, i.e., $\|\mathbf{f}_\theta(\mathbf{x}_1, t, s) - \mathbf{f}_\theta(\mathbf{x}_2, t, s)\|_2 \leq L \|\mathbf{x}_1 - \mathbf{x}_2\|_2$ for all $\mathbf{x}_1, \mathbf{x}_2 \in \mathbb{R}^n$, $t, s \in [0, 1]$. Then, for each fixed $[a, b] \subseteq [0, 1]$ with $b - a$ sufficiently small, if $\mathcal{L}_{\text{STEE}}(\theta)$ reaches its minimum, we have $\mathbf{f}_\theta(\mathbf{x}_t, t, s) = \mathbf{f}(\mathbf{x}_t, t, s)$ for any $[t, s] \subseteq [a, b]$.*

Remark 4. There are notable differences between variants that estimate the interior or end point. As illustrated in Fig. 1 (a), the estimation direction of $\hat{\mathbf{x}}_r$ aligns with the direction from \mathbf{x}_t to \mathbf{x}_s . Consequently, Theorem 2 states that we can fix t and progressively move s further away. In contrast, for variant (b), the direction between $\hat{\mathbf{x}}_t$ estimation and secant learning must be opposite. This requires sampling time pairs where t and s can appear in any order for accurate estimation. As a result, Theorem 3 shows that increasing the distance $|s - t|$ is accompanied by expanding the interval where t and s are randomly sampled rather than simply moving s . In short, t and s play symmetric roles in scenario (b), whereas their roles can be asymmetric in scenario (a).

The proofs of the above theorems rely on properties of conditional expectation and techniques related to the Picard-Lindelöf theorem, specifically by constructing a convergent sequence and applying the Banach fixed-point theorem. Detailed proofs of the total four losses are provided in Appendix A. We note that while the proofs only guarantee local accuracy, the expansion to larger time intervals is achieved through a bootstrapping process. We provide illustrations of using $\mathcal{L}_{\text{SDEI}}$ (Eq. (11)) for distillation and $\mathcal{L}_{\text{STEE}}$ (Eq. (15)) for training in Algorithm 1 and Algorithm 2, respectively. And we illustrate the other two in Appendix D.

Comparison with consistency models. To achieve the same objective of fitting the average velocity (the secant), consistency models [33] (MeanFlow [67]) uses differentiation to construct its loss, whereas our method uses integration. With identical model parameterization, the two methods can be viewed as differential and integral counterparts. The above fundamental difference leads to the following distinctive features of secant losses: **i) Local accuracy.** Consistency models rely on either difference-based approximations of derivatives or explicit derivative terms in their loss functions, which can lead to training instability. In contrast, our loss functions do not involve explicit derivatives, and the solution is accurate when s is near to t .

Table 1: Cost comparison among diffusion loss and secant losses.

Loss	Teacher	#Forward	#Backward
$\mathcal{L}_{\text{Diff}}$	✗	1	1
$\mathcal{L}_{\text{SDEI}}$	✓	3	1
$\mathcal{L}_{\text{STEI}}$	✗	4	2
$\mathcal{L}_{\text{SDEE}}$	✓	3	1
$\mathcal{L}_{\text{STEE}}$	✗	2	1

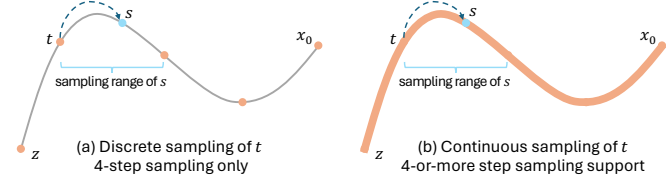


Figure 4: Discrete vs. continuous sampling of t when estimating the interior point.

ii) *Target stability*. We refer to the stability of the prediction target in the loss function as target stability. Under the flow matching interpolant and model parametrization Eq. (5), we compare diffusion loss Eq. 1, secant losses and consistency loss [33, 34, 67]

$$\mathcal{L}_{\text{CT}}(\theta) = \|\mathbf{f}_\theta(\mathbf{x}_t, t, s) - (\alpha'_t \mathbf{x}_0 + \sigma'_t \mathbf{z} + (s-t) \frac{d}{dt} \mathbf{f}_{\theta-}(\mathbf{x}_t, t, s))\|_2 \quad (16)$$

and

$$\mathcal{L}_{\text{CD}}(\theta) = \|\mathbf{f}_\theta(\mathbf{x}_t, t, s) - (\mathbf{v}(\mathbf{x}_t, t) + (s-t) \frac{d}{dt} \mathbf{f}_{\theta-}(\mathbf{x}_t, t, s))\|_2, \quad (17)$$

where CT and CD stand for consistency training and consistency distillation, respectively. One can see that in consistency losses, the item $\frac{d}{dt} \mathbf{f}_{\theta-}(\mathbf{x}_t, t, s)$ (or its discrete version $\frac{\mathbf{f}_{\theta-}(\mathbf{x}_t, t, s) - \mathbf{f}_{\theta-}(\mathbf{x}_{t-\Delta t}, t, s)}{\Delta t}$) is model-dependent and susceptible to numerical issues, which contributes to training instability. In stark contrast, the target of secant losses is either identical to the target of diffusion losses ($\alpha'_t \mathbf{x}_0 + \sigma'_t \mathbf{z}$), or the diffusion model itself ($\mathbf{v}(\mathbf{x}_t, t)$). We illustrate the standard deviation of different losses across training iterations in Fig. 3. This intrinsic target stability provides a compelling explanation for the robust training performance observed with secant losses.

4.3 Practical Choices

Our proposed method is designed for simplicity and robustness, mirroring the design of standard diffusion models. In general it uses: i) A simple time sampling strategy (following diffusion models), ii) a standard loss weighting (following diffusion models), iii) a simple Mean Squared Error (MSE) loss (following diffusion models), iv) a stable loss target discussed in Section 4.2. The strong parallels between our method and standard diffusion models provide a powerful cue: if a standard diffusion model loss works well on a given dataset, it is highly likely our secant losses will too. Here we will discuss more practical designs in application.

Diffusion initialization. As explained in Remark 4, we can use a pretrained diffusion model as the initialization such that $\mathbf{f}_\theta(\mathbf{x}_t, t, t) = \mathbf{v}(\mathbf{x}_t, t)$, which largely accelerates the learning process.

Application of classifier-free guidance (CFG) [68]. For all the secant losses except $\mathcal{L}_{\text{STEE}}$, we can embed CFG as an additional input into the model [22]. Specifically, in the loss functions we substitute $\mathbf{v}(\mathbf{x}_t, t)$ with

$$\mathbf{v}^g(\mathbf{x}_t, t) = \mathbf{v}^u(\mathbf{x}_t, t) + w(\mathbf{v}^c(\mathbf{x}_t, t) - \mathbf{v}^u(\mathbf{x}_t, t)), \quad (18)$$

where w is the guidance scale, and the superscripts g , u and c stand for the model with guidance, the unconditional model and the conditional model, respectively. In contrast, the treatment to $\mathcal{L}_{\text{STEE}}$ is similar to training diffusion models. We can train unconditional and conditional models by randomly dropping the class label, and apply CFG at inference via

$$\mathbf{f}_\theta^g(\mathbf{x}_t, t, s) = \mathbf{f}_\theta^u(\mathbf{x}_t, t, s) + w(\mathbf{f}_\theta^c(\mathbf{x}_t, t, s) - \mathbf{f}_\theta^u(\mathbf{x}_t, t, s)). \quad (19)$$

Step intervals at each sampling step. Adjusting the step intervals may lead to better performance [6, 18]. While for simplicity, we always use uniform sampling steps. Specifically, if the number of steps

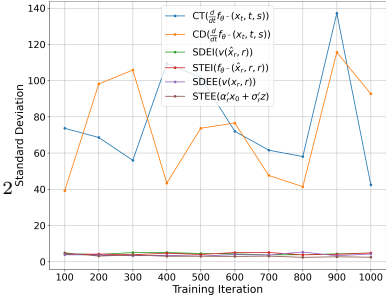


Figure 3: Standard deviation of inspected terms over training iterations. The label format follows *loss type (inspected term)*. The target stability of secant losses is significantly better than that of consistency losses.

is N , then the steps (t, s) are $(\frac{N-i}{N}, \frac{N-i-1}{N})$, $i = 0, \dots, N-1$. We provide details of sampling in Appendix F.

The sampling of t and s when estimating the interior point. Theorem 2 states that we can fix t and randomly sample s . This enables few-step inference at a fixed step count N by setting $t \in \{1, \frac{N-1}{N}, \dots, \frac{i}{N}, \dots, \frac{1}{N}, 0\}$ in training. When $t = \frac{i}{N}$, we randomly sample $s \in [\frac{i-1}{N}, \frac{i}{N}]$. However, this approach constrains us to using exactly N steps during inference. Figure 4 (a) illustrates this with an example where $N = 4$. If we attempt to use more NFEs, such as $2N$, we cannot determine the value of $\mathbf{f}_\theta(\mathbf{x}_{\frac{2N-1}{2N}}, \frac{2N-1}{2N}, \frac{2N-2}{2N})$ at the second step, as the model was not trained with $t = \frac{2N-1}{2N}$. Similarly, with fewer NFEs, such as $\frac{N}{2}$, we cannot compute $\mathbf{f}_\theta(\mathbf{x}_1, 1, \frac{N-2}{N})$ because the case where $t = 1$ and $s = \frac{N-2}{N}$ was not included in training. To enable a flexible step-accuracy trade-off in $\mathcal{L}_{\text{SDEI}}$, we should continuously sample t , as shown in Figure 4 (b). This approach allows inference with any number of NFEs greater than N . Furthermore, if the model is required to perform inversion from images back to Gaussian noise, we should incorporate cases of $s < t$ during training. The sampling strategy of t and s can be chosen according to specific application requirements, due to the limited model capacity. However, for variants that estimate the end point, the sampling of t and s must be both continuous and bidirectional.

The sampling of r . In Eq. (8), we can alter the sampling distribution of r by

$$\begin{aligned} \mathbf{f}(\mathbf{x}_t, t, s) &= \int_t^s \mathbf{v}(\mathbf{x}_r, r) p_{\mathcal{U}(t,s)}(r) dr \\ &= \int_t^s \mathbf{v}(\mathbf{x}_r, r) \frac{p_{\mathcal{U}(t,s)}(r)}{q(r)} q(r) dr \\ &= \mathbb{E}_{r \sim q(r)} \mathbf{v}(\mathbf{x}_r, r) \frac{p_{\mathcal{U}(t,s)}(r)}{q(r)}, \end{aligned} \quad (20)$$

where $q(r)$ is another probability density function that has positive density value within the limits of integration. This means we can unevenly sample r based on the importance, *i.e.*, how we allocate the training effort across different time intervals. We note that while importance sampling can reduce variance, it is not the focus of our paper. The method used in this paper to reduce variance is to employ a stable target.

Resource costs. As the loss formulations suggest, compared to the diffusion loss $\mathcal{L}_{\text{Diff}}$, our proposed loss functions require additional computational resources for forward evaluation and/or backward propagation. We summarize the computational costs in Table 1, and test the practical usage in Appendix G.2.

5 Experiments

In this section, we first compare our method with other related approaches. Subsequently, we conduct ablation studies to validate the design choices of the proposed loss functions.

5.1 Implementation Details

We conduct experiments on common used image generation datasets including CIFAR-10 [37] and ImageNet-256 \times 256 [38]. For quantitative evaluation, we employ the Fréchet Inception Distance (FID) [87] score for both datasets, with additional Inception Score (IS) metric for ImageNet-256 \times 256. There are UNet-based EDM [6] and transformer-based DiT [7] models involved in the experiments, and we load the pretrained weights of EDM and SiT [39] for the two models respectively. More details can be found in Appendix H.

5.2 Main Results

Overall Comparison. We conduct a comprehensive comparison among various few-step diffusion approaches, including fast samplers, few-step distillation, and few-step training/fine-tuning methods. The results are summarized in Tables 2 and 3. On CIFAR-10, our SDEI variant achieves intermediate performance between faster samplers and few-step distillation/training methods. Although

Table 2: Unconditional image generation on CIFAR-10.

Method	FID \downarrow	Steps \downarrow
Diffusion		
DDPM [2]	3.17	1000
Score SDE (deep) [4]	2.20	2000
EDM [6] (Teacher)	1.97	35
Flow Matching [65]	6.35	142
Rectified Flow [47]	2.58	127
Fast Samplers		
DPM-Solver [15]	4.70	10
DPM-Solver++ [16]	2.91	10
DPM-Solver-v3 [17]	2.51	10
DEIS [54]	4.17	10
UniPC [55]	3.87	10
LD3 [64]	2.38	10
Joint Training		
Diff-Instruct [29]	4.53	1
DMD [27]	3.77	1
CTM [34]	1.87	2
SiD [43]	1.92	1
SiD ² A [69]	1.5	1
SiM [70]	2.06	1
Few-step Distillation		
KD [19]	9.36	1
PD [21]	4.51	2
DFNO [20]	3.78	1
2-Rectified Flow [47]	4.85	1
TRACT [71]	3.32	2
PID [72]	3.92	1
CD [33]	2.93	2
sCD [35]	2.52	2
Few-step Training/Tuning		
iCT [73]	2.46	2
ECT [45]	2.11	2
sCT [35]	2.06	2
IMM [74]	1.98	2
SDEI (Ours)	3.23	4
	2.14	10

Table 3: Class-conditional results on ImageNet-256 \times 256.

Method	FID \downarrow	IS \uparrow	Steps \downarrow	#Params
Diffusion				
ADM [5]	10.94	100.98	250	554M
CDM [75]	4.88	158.71	8100	-
SimDiff [76]	2.77	211.8	512	2B
LDM-4 [8]	3.60	247.67	250	400M
U-DiT-L [77]	3.37	246.03	250	916M
U-ViT-H [78]	2.29	263.88	50	501M
DiT-XL/2 [7]	2.27	278.24	250	675M
SiT-XL/2 [39] (Teacher)	2.15	258.09	250	675M
Fast Samplers				
Flow-DPM-Solver [79, 16]	3.76	241.18	8	675M
UniPC [55]	7.51	-	10	-
LD3 [64]	4.32	-	7	-
GAN				
BigGAN [80]	6.95	171.4	1	112M
GigaGAN [81]	3.45	225.52	1	590M
StyleGAN-XL [82]	2.30	265.12	1	166M
Masked and AR				
VQGAN [83]	15.78	78.3	1024	227M
MaskGIT [84]	6.18	182.1	8	227M
MAR-H [85]	1.55	303.7	256	943M
VAR-d30 [86]	1.97	334.7	10	2B
Few-step Training/Tuning				
iCT [73]	20.3	-	2	675M
Shortcut Models [46]	7.80	-	4	675M
IMM (XL/2) [74]	7.77	-	1	675M
	3.99	-	2	675M
	2.51	-	4	675M
	1.99	-	8	675M
STEI (Ours)	7.12	241.75	1	675M
	4.41	242.00	2	675M
	2.78	269.87	4	675M
+guidance interval [40]	2.27	273.76	4	675M
	2.36	247.72	8	675M
+guidance interval [40]	1.96	276.12	8	675M
STEE (Ours)	3.02	274.00	4	675M
+guidance interval [40]	2.55	275.83	4	675M
	2.33	274.47	8	675M
+guidance interval [40]	1.96	275.81	8	675M

consistency models [33, 45, 34, 35] demonstrate superior performance on this dataset, we observe training instability issues. More notably, when scaling to ImageNet-256 \times 256 with greater data variation, these models diverge in our experiments³. In contrast, our proposed loss functions exhibit consistent stability and rapid convergence, enabling efficient model distillation or fine-tuning that requires merely 1% of the original SiT training duration (50K \sim 100K versus 7M iterations). On the larger-scale ImageNet-256 \times 256 dataset, our approach consistently outperforms fast samplers and ranks second only to the recent IMM [74] in both 4-step and 8-step settings. Notably, for one-step generation, STEI even surpasses both IMM and 4-step Shortcut Models [46]. By incorporating interval CFG [40], our method further achieves a 4-step FID of 2.27 and an 8-step FID of 1.96, where we simply ignore the guidance for the first step in 4-step generation and the first two steps in 8-step generation. Fig. 2 showcases generated samples using 8 steps on ImageNet-256 \times 256 with our best-performing model. While both effective, our method differs from IMM: ours is grounded in the

³Due to training divergence of consistency models, we cite the iCT [73] result reported in [74].

Table 4: The effect of the weighting factor λ in $\mathcal{L}_{\text{STEI}}$ on ImageNet-256 \times 256 with 4 sampling steps.

λ	FID \downarrow	IS \uparrow
0.1	3.96	206.14
0.5	3.15	232.15
1.0	2.84	249.57
2.0	3.96	213.56

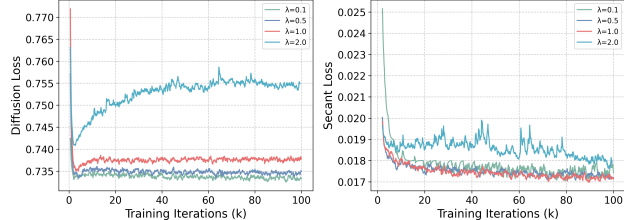


Figure 5: The effect of λ in $\mathcal{L}_{\text{STEI}}$ on training dynamics.

exact solution of the PF-ODE (therefore the performance of our models is bounded by the teacher model SiT[39]), whereas IMM relies on distribution-level losses [88]. For classifier-free guidance, IMM follows Eq. (19), while STEI applies the integral-form CFG following Eq. (18). This difference may explain our superior performance in one-step generation.

Comparison of secant losses. We evaluate the four types of secant losses proposed in Section 4 on CIFAR-10 and ImageNet-256 \times 256 datasets. The result can be found at Table 7 in Appendix G. In the absence of classifier-free guidance, similar trends emerge across both datasets. The distillation variants generally demonstrate superior performance compared to the training counterparts, with the exception of STEI on ImageNet-256 \times 256. Furthermore, variants with interior-point estimation perform better and degrade more slowly as the step number decreases, which can be explained by three aspects: i) Input correctness. For inner-point variants, the input to the training network is the clean data \mathbf{x}_t , while in end-point variants, the input is the estimated $\hat{\mathbf{x}}_r$. Fitting a fixed, clean input distribution, is more efficient than fitting an input dependent of the model historical output. ii) Error accumulation path, *i.e.*, the path from clean data to the prediction destination. In inner-point variants, the path is $\mathbf{x}_t \rightarrow \mathbf{x}_s$, while in end-point variants it is $\mathbf{x}_r \rightarrow \mathbf{x}_t \rightarrow \mathbf{x}_s$. Generally, the path in end-point variants is longer than that in inner-point variants. iii) Model capacity. As per Fig. 1 and Algorithm 2, the end-point variants additionally require inversion, which costs part of the model capacity. With classifier guidance applied, the performance gap narrows on ImageNet-256 \times 256, with the STEE variant achieving the best 8-step FID of 2.33. Based on the computational costs presented in Table 1, we recommend using $\mathcal{L}_{\text{SDEI}}$ for distillation and $\mathcal{L}_{\text{STEE}}$ for training. These variants offer optimal performance while minimizing both computational time and GPU memory requirements compared to other methods.

5.3 Ablations

The loss weighting in $\mathcal{L}_{\text{STEI}}$. We investigate the balancing factor λ in $\mathcal{L}_{\text{STEI}}$, which comprises the diffusion loss and the secant loss. Figure 5 illustrates the training dynamics of both losses (excluding the λ factor in the secant loss). When λ increases from 0.1 to 1.0, we observe a reduction in the secant loss while maintaining relatively stable diffusion loss levels. However, at $\lambda = 2$, the model exhibits significant deterioration in diffusion loss, accompanied by increased instability in the secant loss. The quantitative results presented in Table 4 confirm that $\lambda = 1$ achieves the optimal balance, yielding the best overall performance.

The sampling of t and s in interior-point estimation. As shown in Fig. 4, $\mathcal{L}_{\text{SDEI}}$ and $\mathcal{L}_{\text{STEI}}$ offer flexibility in sampling the time point t and s during training. Given the fixed model capacity, different sampling strategies lead to varying performance characteristics. For fixed N -step generation, discrete sampling suffices; to enable step-performance trade-off, continuous sampling of t becomes necessary; to incorporate the capability of inversion, bidirectional sampling ($t < s$ and $t > s$) is required. The results in Table 5 demonstrate that the best performance is achieved with the discrete sampling and generation-only configuration (first row), and each additional functionality comes at the cost of decreased performance.

Table 5: The effect of t, s sampling on CIFAR-10 with 4 steps.

Gen.	Inv.	t sampling	FID \downarrow
✓	✗	discrete	3.23
✓	✓	discrete	3.63
✓	✗	continuous	4.29
✓	✓	continuous	5.47

The sampling of r . Following Eq. (20), we know that we can use alternative distributions $q(r)$ to sample r . Here we investigate sampling strategies for r . The cases include standard uniform sampling and biased sampling schemes that favor positions closer to t , s or the midpoint $\frac{s+t}{2}$. These biased sampling strategies are implemented using truncated normal distributions, denoted as $\mathcal{T}\mathcal{N}(\mu, \sigma, a, b)$ where μ represents the mean, σ the standard deviation, and $[a, b]$ the truncated interval. Details are provided in Appendix E. As the results in Table 6 indicates, all sampling strategies works comparable, and the uniform strategy works slightly better than others.

Training from scratch. We evaluate the scalability and from-scratch training capabilities of the secant loss using $\mathcal{L}_{\text{STEE}}$ as the representative loss function. We conduct experiments with varying model capacities, including DiT-S/2, DiT-B/2, DiT-L/2 and DiT-XL/2. Figure 6 presents the evolution of FID scores during the first 1000K training iterations, with a guidance scale of 1.5 used at sampling phase. The results clearly show a correlation between model capacity and generation quality, with larger architectures consistently achieving superior performance. After extending the training to 3000K iterations, our DiT-XL/2 model achieves an 8-step FID of 2.68, which is slightly higher than the fine-tuning FID. This is expected, given that the training period of the teacher model SiT [39] (7000K iterations) is significantly longer than our training duration.

6 Limitations

While our method can stably and rapidly convert a diffusion model into a few-step generator, there is still a significant performance gap between 1-step and 8-step generation. Additionally, the performance on ImageNet 256×256 relies heavily on classifier-free guidance, and the theoretical relationship between CFG and secant losses may be explored in future work. Lastly, our method requires training data, which may present constraints in data-limited scenarios.

7 Conclusion

In this paper, we introduce a novel family of loss functions, termed secant losses, that efficiently learn to integrate diffusion ODEs through Monte Carlo integration and Picard iteration. Our proposed losses operate by estimating and averaging tangents to learn the corresponding secants. We present both theoretical and intuitive interpretations of these secant losses, and empirically demonstrate their robustness and efficiency on CIFAR-10 and ImageNet 256×256 datasets.

Acknowledgments

This work is partially supported by the National Natural Science Foundation of China (Grant No. 62306261), and The Shun Hing Institute of Advanced Engineering (SHIAE) Grant (No. 8115074). This study was supported in part by the Centre for Perceptual and Interactive Intelligence, a CUHK-led InnoCentre under the InnoHK initiative of the Innovation and Technology Commission of the Hong Kong Special Administrative Region Government. This work is also partially supported by Hong Kong RGC Strategic Topics Grant STG1/E-403/24-N, and CUHK-CUHK(SZ)-GDST Joint Collaboration Fund YSP26-4760949.

References

[1] Jascha Sohl-Dickstein, Eric Weiss, Niru Maheswaranathan, and Surya Ganguli. Deep unsupervised learning using nonequilibrium thermodynamics. In *International conference on machine learning*, pages 2256–2265. pmlr, 2015.

Table 6: 4-step results of different r distributions on ImageNet- 256×256 with $\mathcal{L}_{\text{SDEI}}$. We first sample \tilde{r} , and obtain $r = t + (s - t)\tilde{r}$.

\tilde{r} distribution	FID \downarrow	IS \uparrow
$\mathcal{U}(0, 1)$	3.57	222.83
$\mathcal{T}\mathcal{N}(0, 0.5, 0, 1)$	3.84	215.57
$\mathcal{T}\mathcal{N}(0.5, 0.5, 0, 1)$	3.59	221.44
$\mathcal{T}\mathcal{N}(1, 0.5, 0, 1)$	3.71	216.93

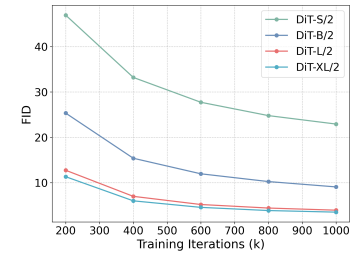


Figure 6: Results of training from scratch on ImageNet- 256×256 . The guidance scale is 1.5.

- [2] Jonathan Ho, Ajay Jain, and Pieter Abbeel. Denoising diffusion probabilistic models. *Advances in neural information processing systems*, 33:6840–6851, 2020.
- [3] Yang Song and Stefano Ermon. Generative modeling by estimating gradients of the data distribution. *Advances in neural information processing systems*, 32, 2019.
- [4] Yang Song, Jascha Sohl-Dickstein, Diederik P Kingma, Abhishek Kumar, Stefano Ermon, and Ben Poole. Score-based generative modeling through stochastic differential equations. *arXiv preprint arXiv:2011.13456*, 2020.
- [5] Prafulla Dhariwal and Alexander Nichol. Diffusion models beat gans on image synthesis. *Advances in neural information processing systems*, 34:8780–8794, 2021.
- [6] Tero Karras, Miika Aittala, Timo Aila, and Samuli Laine. Elucidating the design space of diffusion-based generative models. *Advances in neural information processing systems*, 35:26565–26577, 2022.
- [7] William Peebles and Saining Xie. Scalable diffusion models with transformers. In *Proceedings of the IEEE/CVF international conference on computer vision*, pages 4195–4205, 2023.
- [8] Robin Rombach, Andreas Blattmann, Dominik Lorenz, Patrick Esser, and Björn Ommer. High-resolution image synthesis with latent diffusion models. In *Proceedings of the IEEE/CVF conference on computer vision and pattern recognition*, pages 10684–10695, 2022.
- [9] Andreas Blattmann, Robin Rombach, Huan Ling, Tim Dockhorn, Seung Wook Kim, Sanja Fidler, and Karsten Kreis. Align your latents: High-resolution video synthesis with latent diffusion models. In *Proceedings of the IEEE/CVF conference on computer vision and pattern recognition*, pages 22563–22575, 2023.
- [10] Jonathan Ho, Tim Salimans, Alexey Gritsenko, William Chan, Mohammad Norouzi, and David J Fleet. Video diffusion models. *Advances in Neural Information Processing Systems*, 35:8633–8646, 2022.
- [11] Andreas Blattmann, Tim Dockhorn, Sumith Kulal, Daniel Mendelevitch, Maciej Kilian, Dominik Lorenz, Yam Levi, Zion English, Vikram Voleti, Adam Letts, et al. Stable video diffusion: Scaling latent video diffusion models to large datasets. *arXiv preprint arXiv:2311.15127*, 2023.
- [12] Zhipeng Kong, Wei Ping, Jiaji Huang, Kexin Zhao, and Bryan Catanzaro. Diffwave: A versatile diffusion model for audio synthesis. *arXiv preprint arXiv:2009.09761*, 2020.
- [13] Rongjie Huang, Jiawei Huang, Dongchao Yang, Yi Ren, Luping Liu, Mingze Li, Zhenhui Ye, Jinglin Liu, Xiang Yin, and Zhou Zhao. Make-an-audio: Text-to-audio generation with prompt-enhanced diffusion models. In *International Conference on Machine Learning*, pages 13916–13932. PMLR, 2023.
- [14] Haohe Liu, Zehua Chen, Yi Yuan, Xinhao Mei, Xubo Liu, Danilo Mandic, Wenwu Wang, and Mark D Plumbley. Audioldm: Text-to-audio generation with latent diffusion models. *arXiv preprint arXiv:2301.12503*, 2023.
- [15] Cheng Lu, Yuhao Zhou, Fan Bao, Jianfei Chen, Chongxuan Li, and Jun Zhu. Dpm-solver: A fast ode solver for diffusion probabilistic model sampling in around 10 steps. *Advances in Neural Information Processing Systems*, 35:5775–5787, 2022.
- [16] Cheng Lu, Yuhao Zhou, Fan Bao, Jianfei Chen, Chongxuan Li, and Jun Zhu. Dpm-solver++: Fast solver for guided sampling of diffusion probabilistic models. *arXiv preprint arXiv:2211.01095*, 2022.
- [17] Kaiwen Zheng, Cheng Lu, Jianfei Chen, and Jun Zhu. Dpm-solver-v3: Improved diffusion ode solver with empirical model statistics. *Advances in Neural Information Processing Systems*, 36:55502–55542, 2023.
- [18] Daniel Watson, William Chan, Jonathan Ho, and Mohammad Norouzi. Learning fast samplers for diffusion models by differentiating through sample quality. In *International Conference on Learning Representations*, 2021.

[19] Eric Luhman and Troy Luhman. Knowledge distillation in iterative generative models for improved sampling speed. *arXiv preprint arXiv:2101.02388*, 2021.

[20] Hongkai Zheng, Weili Nie, Arash Vahdat, Kamyar Azizzadenesheli, and Anima Anandkumar. Fast sampling of diffusion models via operator learning. In *International conference on machine learning*, pages 42390–42402. PMLR, 2023.

[21] Tim Salimans and Jonathan Ho. Progressive distillation for fast sampling of diffusion models. *arXiv preprint arXiv:2202.00512*, 2022.

[22] Chenlin Meng, Robin Rombach, Ruiqi Gao, Diederik Kingma, Stefano Ermon, Jonathan Ho, and Tim Salimans. On distillation of guided diffusion models. In *Proceedings of the IEEE/CVF Conference on Computer Vision and Pattern Recognition*, pages 14297–14306, 2023.

[23] Axel Sauer, Dominik Lorenz, Andreas Blattmann, and Robin Rombach. Adversarial diffusion distillation. In *European Conference on Computer Vision*, pages 87–103. Springer, 2024.

[24] Zhendong Wang, Huangjie Zheng, Pengcheng He, Weizhu Chen, and Mingyuan Zhou. Diffusion-gan: Training gans with diffusion. *arXiv preprint arXiv:2206.02262*, 2022.

[25] Axel Sauer, Frederic Boesel, Tim Dockhorn, Andreas Blattmann, Patrick Esser, and Robin Rombach. Fast high-resolution image synthesis with latent adversarial diffusion distillation. In *SIGGRAPH Asia 2024 Conference Papers*, pages 1–11, 2024.

[26] Zhengyi Wang, Cheng Lu, Yikai Wang, Fan Bao, Chongxuan Li, Hang Su, and Jun Zhu. Pro-lificdreamer: High-fidelity and diverse text-to-3d generation with variational score distillation. *Advances in Neural Information Processing Systems*, 36:8406–8441, 2023.

[27] Tianwei Yin, Michaël Gharbi, Richard Zhang, Eli Shechtman, Fredo Durand, William T Freeman, and Taesung Park. One-step diffusion with distribution matching distillation. In *Proceedings of the IEEE/CVF conference on computer vision and pattern recognition*, pages 6613–6623, 2024.

[28] Tianwei Yin, Michaël Gharbi, Taesung Park, Richard Zhang, Eli Shechtman, Fredo Durand, and Bill Freeman. Improved distribution matching distillation for fast image synthesis. *Advances in Neural Information Processing Systems*, 37:47455–47487, 2025.

[29] Weijian Luo, Tianyang Hu, Shifeng Zhang, Jiacheng Sun, Zhenguo Li, and Zhihua Zhang. Diff-instruct: A universal approach for transferring knowledge from pre-trained diffusion models. *Advances in Neural Information Processing Systems*, 36:76525–76546, 2023.

[30] Weijian Luo, Colin Zhang, Debing Zhang, and Zhengyang Geng. Diff-instruct*: Towards human-preferred one-step text-to-image generative models. *arXiv preprint arXiv:2410.20898*, 2024.

[31] Sirui Xie, Zhisheng Xiao, Diederik P Kingma, Tingbo Hou, Ying Nian Wu, Kevin Patrick Murphy, Tim Salimans, Ben Poole, and Ruiqi Gao. Em distillation for one-step diffusion models. *arXiv preprint arXiv:2405.16852*, 2024.

[32] Tim Salimans, Thomas Mensink, Jonathan Heek, and Emiel Hoogeboom. Multistep distillation of diffusion models via moment matching. *Advances in Neural Information Processing Systems*, 37:36046–36070, 2025.

[33] Yang Song, Prafulla Dhariwal, Mark Chen, and Ilya Sutskever. Consistency models. *arXiv preprint arXiv:2303.01469*, 2023.

[34] Dongjun Kim, Chieh-Hsin Lai, Wei-Hsiang Liao, Naoki Murata, Yuhta Takida, Toshimitsu Uesaka, Yutong He, Yuki Mitsufuji, and Stefano Ermon. Consistency trajectory models: Learning probability flow ode trajectory of diffusion. *arXiv preprint arXiv:2310.02279*, 2023.

[35] Cheng Lu and Yang Song. Simplifying, stabilizing and scaling continuous-time consistency models. *arXiv preprint arXiv:2410.11081*, 2024.

[36] Nicholas M Boffi, Michael S Albergo, and Eric Vanden-Eijnden. Flow map matching. *arXiv preprint arXiv:2406.07507*, 2024.

[37] Alex Krizhevsky, Geoffrey Hinton, et al. Learning multiple layers of features from tiny images. 2009.

[38] Jia Deng, Wei Dong, Richard Socher, Li-Jia Li, Kai Li, and Li Fei-Fei. Imagenet: A large-scale hierarchical image database. In *2009 IEEE conference on computer vision and pattern recognition*, pages 248–255. Ieee, 2009.

[39] Nanye Ma, Mark Goldstein, Michael S Albergo, Nicholas M Boffi, Eric Vanden-Eijnden, and Saining Xie. Sit: Exploring flow and diffusion-based generative models with scalable interpolant transformers. In *European Conference on Computer Vision*, pages 23–40. Springer, 2024.

[40] Tuomas Kynkänniemi, Miika Aittala, Tero Karras, Samuli Laine, Timo Aila, and Jaakko Lehtinen. Applying guidance in a limited interval improves sample and distribution quality in diffusion models. *arXiv preprint arXiv:2404.07724*, 2024.

[41] Geoffrey Hinton, Oriol Vinyals, and Jeff Dean. Distilling the knowledge in a neural network. *arXiv preprint arXiv:1503.02531*, 2015.

[42] Ian Goodfellow, Jean Pouget-Abadie, Mehdi Mirza, Bing Xu, David Warde-Farley, Sherjil Ozair, Aaron Courville, and Yoshua Bengio. Generative adversarial nets. *Advances in neural information processing systems*, 27, 2014.

[43] Mingyuan Zhou, Huangjie Zheng, Zhendong Wang, Mingzhang Yin, and Hai Huang. Score identity distillation: Exponentially fast distillation of pretrained diffusion models for one-step generation. In *Forty-first International Conference on Machine Learning*, 2024.

[44] Zemin Huang, Zhengyang Geng, Weijian Luo, and Guo-jun Qi. Flow generator matching. *arXiv preprint arXiv:2410.19310*, 2024.

[45] Zhengyang Geng, Ashwini Pokle, William Luo, Justin Lin, and J Zico Kolter. Consistency models made easy. *arXiv preprint arXiv:2406.14548*, 2024.

[46] Kevin Frans, Danijar Hafner, Sergey Levine, and Pieter Abbeel. One step diffusion via shortcut models. *arXiv preprint arXiv:2410.12557*, 2024.

[47] Xingchao Liu, Chengyue Gong, and Qiang Liu. Flow straight and fast: Learning to generate and transfer data with rectified flow. *arXiv preprint arXiv:2209.03003*, 2022.

[48] Xingchao Liu, Xiwen Zhang, Jianzhu Ma, Jian Peng, et al. Instaflow: One step is enough for high-quality diffusion-based text-to-image generation. In *The Twelfth International Conference on Learning Representations*, 2023.

[49] Jiaming Song, Chenlin Meng, and Stefano Ermon. Denoising diffusion implicit models. *arXiv preprint arXiv:2010.02502*, 2020.

[50] Alexia Jolicoeur-Martineau, Ke Li, Rémi Piché-Taillefer, Tal Kachman, and Ioannis Mitliagkas. Gotta go fast when generating data with score-based models. *arXiv preprint arXiv:2105.14080*, 2021.

[51] Zhifeng Kong and Wei Ping. On fast sampling of diffusion probabilistic models. *arXiv preprint arXiv:2106.00132*, 2021.

[52] Fan Bao, Chongxuan Li, Jun Zhu, and Bo Zhang. Analytic-dpm: an analytic estimate of the optimal reverse variance in diffusion probabilistic models. *arXiv preprint arXiv:2201.06503*, 2022.

[53] Qinsheng Zhang, Molei Tao, and Yongxin Chen. gddim: Generalized denoising diffusion implicit models. *arXiv preprint arXiv:2206.05564*, 2022.

[54] Qinsheng Zhang and Yongxin Chen. Fast sampling of diffusion models with exponential integrator. *arXiv preprint arXiv:2204.13902*, 2022.

[55] Wenliang Zhao, Lujia Bai, Yongming Rao, Jie Zhou, and Jiwen Lu. Unipc: A unified predictor-corrector framework for fast sampling of diffusion models. *Advances in Neural Information Processing Systems*, 36:49842–49869, 2023.

[56] Andy Shih, Suneel Belkhale, Stefano Ermon, Dorsa Sadigh, and Nima Anari. Parallel sampling of diffusion models. *Advances in Neural Information Processing Systems*, 36:4263–4276, 2023.

[57] Zhiwei Tang, Jiasheng Tang, Hao Luo, Fan Wang, and Tsung-Hui Chang. Accelerating parallel sampling of diffusion models. In *Forty-first International Conference on Machine Learning*, 2024.

[58] Fan Bao, Chongxuan Li, Jiacheng Sun, Jun Zhu, and Bo Zhang. Estimating the optimal covariance with imperfect mean in diffusion probabilistic models. *arXiv preprint arXiv:2206.07309*, 2022.

[59] Tim Dockhorn, Arash Vahdat, and Karsten Kreis. Genie: Higher-order denoising diffusion solvers. *Advances in Neural Information Processing Systems*, 35:30150–30166, 2022.

[60] Zhenyu Zhou, Defang Chen, Can Wang, and Chun Chen. Fast ode-based sampling for diffusion models in around 5 steps. In *Proceedings of the IEEE/CVF Conference on Computer Vision and Pattern Recognition*, pages 7777–7786, 2024.

[61] Amirmojtaba Sabour, Sanja Fidler, and Karsten Kreis. Align your steps: Optimizing sampling schedules in diffusion models. *arXiv preprint arXiv:2404.14507*, 2024.

[62] Defang Chen, Zhenyu Zhou, Can Wang, Chunhua Shen, and Siwei Lyu. On the trajectory regularity of ode-based diffusion sampling. *arXiv preprint arXiv:2405.11326*, 2024.

[63] Shuchen Xue, Zhaoqiang Liu, Fei Chen, Shifeng Zhang, Tianyang Hu, Enze Xie, and Zhenguo Li. Accelerating diffusion sampling with optimized time steps. In *Proceedings of the IEEE/CVF Conference on Computer Vision and Pattern Recognition*, pages 8292–8301, 2024.

[64] Vinh Tong, Trung-Dung Hoang, Anji Liu, Guy Van den Broeck, and Mathias Niepert. Learning to discretize denoising diffusion odes. *arXiv preprint arXiv:2405.15506*, 2024.

[65] Yaron Lipman, Ricky TQ Chen, Heli Ben-Hamu, Maximilian Nickel, and Matt Le. Flow matching for generative modeling. *arXiv preprint arXiv:2210.02747*, 2022.

[66] Michael S Albergo, Nicholas M Boffi, and Eric Vanden-Eijnden. Stochastic interpolants: A unifying framework for flows and diffusions. *arXiv preprint arXiv:2303.08797*, 2023.

[67] Zhengyang Geng, Mingyang Deng, Xingjian Bai, J Zico Kolter, and Kaiming He. Mean flows for one-step generative modeling. *arXiv preprint arXiv:2505.13447*, 2025.

[68] Jonathan Ho and Tim Salimans. Classifier-free diffusion guidance. *arXiv preprint arXiv:2207.12598*, 2022.

[69] Mingyuan Zhou, Huangjie Zheng, Yi Gu, Zhendong Wang, and Hai Huang. Adversarial score identity distillation: Rapidly surpassing the teacher in one step. *arXiv preprint arXiv:2410.14919*, 2024.

[70] Weijian Luo, Zemin Huang, Zhengyang Geng, J Zico Kolter, and Guo-jun Qi. One-step diffusion distillation through score implicit matching. *Advances in Neural Information Processing Systems*, 37:115377–115408, 2024.

[71] David Berthelot, Arnaud Autef, Jierui Lin, Dian Ang Yap, Shuangfei Zhai, Siyuan Hu, Daniel Zheng, Walter Talbott, and Eric Gu. Tract: Denoising diffusion models with transitive closure time-distillation. *arXiv preprint arXiv:2303.04248*, 2023.

[72] Joshua Tian Jin Tee, Kang Zhang, Hee Suk Yoon, Dhananjaya Nagaraja Gowda, Chanwoo Kim, and Chang D Yoo. Physics informed distillation for diffusion models. *arXiv preprint arXiv:2411.08378*, 2024.

[73] Yang Song and Prafulla Dhariwal. Improved techniques for training consistency models. *arXiv preprint arXiv:2310.14189*, 2023.

[74] Linqi Zhou, Stefano Ermon, and Jiaming Song. Inductive moment matching. *arXiv preprint arXiv:2503.07565*, 2025.

[75] Jonathan Ho, Chitwan Saharia, William Chan, David J Fleet, Mohammad Norouzi, and Tim Salimans. Cascaded diffusion models for high fidelity image generation. *Journal of Machine Learning Research*, 23(47):1–33, 2022.

[76] Emiel Hoogeboom, Jonathan Heek, and Tim Salimans. simple diffusion: End-to-end diffusion for high resolution images. In *International Conference on Machine Learning*, pages 13213–13232. PMLR, 2023.

[77] Yuchuan Tian, Zhijun Tu, Hanting Chen, Jie Hu, Chao Xu, and Yunhe Wang. U-dits: Downsample tokens in u-shaped diffusion transformers. *arXiv preprint arXiv:2405.02730*, 2024.

[78] Fan Bao, Shen Nie, Kaiwen Xue, Yue Cao, Chongxuan Li, Hang Su, and Jun Zhu. All are worth words: A vit backbone for diffusion models. In *Proceedings of the IEEE/CVF conference on computer vision and pattern recognition*, pages 22669–22679, 2023.

[79] Enze Xie, Junsong Chen, Junyu Chen, Han Cai, Haotian Tang, Yujun Lin, Zhekai Zhang, Muyang Li, Ligeng Zhu, Yao Lu, et al. Sana: Efficient high-resolution image synthesis with linear diffusion transformers. *arXiv preprint arXiv:2410.10629*, 2024.

[80] Andrew Brock, Jeff Donahue, and Karen Simonyan. Large scale gan training for high fidelity natural image synthesis. *arXiv preprint arXiv:1809.11096*, 2018.

[81] Minguk Kang, Jun-Yan Zhu, Richard Zhang, Jaesik Park, Eli Shechtman, Sylvain Paris, and Taesung Park. Scaling up gans for text-to-image synthesis. In *Proceedings of the IEEE/CVF conference on computer vision and pattern recognition*, pages 10124–10134, 2023.

[82] Axel Sauer, Katja Schwarz, and Andreas Geiger. Stylegan-xl: Scaling stylegan to large diverse datasets. In *ACM SIGGRAPH 2022 conference proceedings*, pages 1–10, 2022.

[83] Patrick Esser, Robin Rombach, and Bjorn Ommer. Taming transformers for high-resolution image synthesis. In *Proceedings of the IEEE/CVF conference on computer vision and pattern recognition*, pages 12873–12883, 2021.

[84] Huiwen Chang, Han Zhang, Lu Jiang, Ce Liu, and William T Freeman. Maskgit: Masked generative image transformer. In *Proceedings of the IEEE/CVF conference on computer vision and pattern recognition*, pages 11315–11325, 2022.

[85] Tianhong Li, Yonglong Tian, He Li, Mingyang Deng, and Kaiming He. Autoregressive image generation without vector quantization. *Advances in Neural Information Processing Systems*, 37:56424–56445, 2024.

[86] Keyu Tian, Yi Jiang, Zehuan Yuan, Bingyue Peng, and Liwei Wang. Visual autoregressive modeling: Scalable image generation via next-scale prediction. *Advances in neural information processing systems*, 37:84839–84865, 2024.

[87] Martin Heusel, Hubert Ramsauer, Thomas Unterthiner, Bernhard Nessler, and Sepp Hochreiter. Gans trained by a two time-scale update rule converge to a local nash equilibrium. *Advances in neural information processing systems*, 30, 2017.

[88] Yujia Li, Kevin Swersky, and Rich Zemel. Generative moment matching networks. In *International conference on machine learning*, pages 1718–1727. PMLR, 2015.

NeurIPS Paper Checklist

1. Claims

Question: Do the main claims made in the abstract and introduction accurately reflect the paper's contributions and scope?

Answer: [\[Yes\]](#)

Justification: We clearly present the contribution and scope.

Guidelines:

- The answer NA means that the abstract and introduction do not include the claims made in the paper.
- The abstract and/or introduction should clearly state the claims made, including the contributions made in the paper and important assumptions and limitations. A No or NA answer to this question will not be perceived well by the reviewers.
- The claims made should match theoretical and experimental results, and reflect how much the results can be expected to generalize to other settings.
- It is fine to include aspirational goals as motivation as long as it is clear that these goals are not attained by the paper.

2. Limitations

Question: Does the paper discuss the limitations of the work performed by the authors?

Answer: [\[Yes\]](#)

Justification: We discuss the limitations in Section 6.

Guidelines:

- The answer NA means that the paper has no limitation while the answer No means that the paper has limitations, but those are not discussed in the paper.
- The authors are encouraged to create a separate "Limitations" section in their paper.
- The paper should point out any strong assumptions and how robust the results are to violations of these assumptions (e.g., independence assumptions, noiseless settings, model well-specification, asymptotic approximations only holding locally). The authors should reflect on how these assumptions might be violated in practice and what the implications would be.
- The authors should reflect on the scope of the claims made, e.g., if the approach was only tested on a few datasets or with a few runs. In general, empirical results often depend on implicit assumptions, which should be articulated.
- The authors should reflect on the factors that influence the performance of the approach. For example, a facial recognition algorithm may perform poorly when image resolution is low or images are taken in low lighting. Or a speech-to-text system might not be used reliably to provide closed captions for online lectures because it fails to handle technical jargon.
- The authors should discuss the computational efficiency of the proposed algorithms and how they scale with dataset size.
- If applicable, the authors should discuss possible limitations of their approach to address problems of privacy and fairness.
- While the authors might fear that complete honesty about limitations might be used by reviewers as grounds for rejection, a worse outcome might be that reviewers discover limitations that aren't acknowledged in the paper. The authors should use their best judgment and recognize that individual actions in favor of transparency play an important role in developing norms that preserve the integrity of the community. Reviewers will be specifically instructed to not penalize honesty concerning limitations.

3. Theory assumptions and proofs

Question: For each theoretical result, does the paper provide the full set of assumptions and a complete (and correct) proof?

Answer: [\[Yes\]](#)

Justification: For Theorem 2 and Theorem 3, we provide the assumptions and proofs in Appendix A.

Guidelines:

- The answer NA means that the paper does not include theoretical results.
- All the theorems, formulas, and proofs in the paper should be numbered and cross-referenced.
- All assumptions should be clearly stated or referenced in the statement of any theorems.
- The proofs can either appear in the main paper or the supplemental material, but if they appear in the supplemental material, the authors are encouraged to provide a short proof sketch to provide intuition.
- Inversely, any informal proof provided in the core of the paper should be complemented by formal proofs provided in appendix or supplemental material.
- Theorems and Lemmas that the proof relies upon should be properly referenced.

4. Experimental result reproducibility

Question: Does the paper fully disclose all the information needed to reproduce the main experimental results of the paper to the extent that it affects the main claims and/or conclusions of the paper (regardless of whether the code and data are provided or not)?

Answer: **[Yes]**

Justification: We provide experimental details in Appendix H.

Guidelines:

- The answer NA means that the paper does not include experiments.
- If the paper includes experiments, a No answer to this question will not be perceived well by the reviewers: Making the paper reproducible is important, regardless of whether the code and data are provided or not.
- If the contribution is a dataset and/or model, the authors should describe the steps taken to make their results reproducible or verifiable.
- Depending on the contribution, reproducibility can be accomplished in various ways. For example, if the contribution is a novel architecture, describing the architecture fully might suffice, or if the contribution is a specific model and empirical evaluation, it may be necessary to either make it possible for others to replicate the model with the same dataset, or provide access to the model. In general, releasing code and data is often one good way to accomplish this, but reproducibility can also be provided via detailed instructions for how to replicate the results, access to a hosted model (e.g., in the case of a large language model), releasing of a model checkpoint, or other means that are appropriate to the research performed.
- While NeurIPS does not require releasing code, the conference does require all submissions to provide some reasonable avenue for reproducibility, which may depend on the nature of the contribution. For example
 - (a) If the contribution is primarily a new algorithm, the paper should make it clear how to reproduce that algorithm.
 - (b) If the contribution is primarily a new model architecture, the paper should describe the architecture clearly and fully.
 - (c) If the contribution is a new model (e.g., a large language model), then there should either be a way to access this model for reproducing the results or a way to reproduce the model (e.g., with an open-source dataset or instructions for how to construct the dataset).
 - (d) We recognize that reproducibility may be tricky in some cases, in which case authors are welcome to describe the particular way they provide for reproducibility. In the case of closed-source models, it may be that access to the model is limited in some way (e.g., to registered users), but it should be possible for other researchers to have some path to reproducing or verifying the results.

5. Open access to data and code

Question: Does the paper provide open access to the data and code, with sufficient instructions to faithfully reproduce the main experimental results, as described in supplemental material?

Answer: [No]

Justification: We only provide the detailed settings and algorithm. We will make the code public in the future.

Guidelines:

- The answer NA means that paper does not include experiments requiring code.
- Please see the NeurIPS code and data submission guidelines (<https://nips.cc/public/guides/CodeSubmissionPolicy>) for more details.
- While we encourage the release of code and data, we understand that this might not be possible, so “No” is an acceptable answer. Papers cannot be rejected simply for not including code, unless this is central to the contribution (e.g., for a new open-source benchmark).
- The instructions should contain the exact command and environment needed to run to reproduce the results. See the NeurIPS code and data submission guidelines (<https://nips.cc/public/guides/CodeSubmissionPolicy>) for more details.
- The authors should provide instructions on data access and preparation, including how to access the raw data, preprocessed data, intermediate data, and generated data, etc.
- The authors should provide scripts to reproduce all experimental results for the new proposed method and baselines. If only a subset of experiments are reproducible, they should state which ones are omitted from the script and why.
- At submission time, to preserve anonymity, the authors should release anonymized versions (if applicable).
- Providing as much information as possible in supplemental material (appended to the paper) is recommended, but including URLs to data and code is permitted.

6. Experimental setting/details

Question: Does the paper specify all the training and test details (e.g., data splits, hyper-parameters, how they were chosen, type of optimizer, etc.) necessary to understand the results?

Answer: [Yes]

Justification: We provide the details in Appendix H.

Guidelines:

- The answer NA means that the paper does not include experiments.
- The experimental setting should be presented in the core of the paper to a level of detail that is necessary to appreciate the results and make sense of them.
- The full details can be provided either with the code, in appendix, or as supplemental material.

7. Experiment statistical significance

Question: Does the paper report error bars suitably and correctly defined or other appropriate information about the statistical significance of the experiments?

Answer: [No]

Justification: Due to limited computing resources, we do not report error bars in the paper.

Guidelines:

- The answer NA means that the paper does not include experiments.
- The authors should answer "Yes" if the results are accompanied by error bars, confidence intervals, or statistical significance tests, at least for the experiments that support the main claims of the paper.
- The factors of variability that the error bars are capturing should be clearly stated (for example, train/test split, initialization, random drawing of some parameter, or overall run with given experimental conditions).
- The method for calculating the error bars should be explained (closed form formula, call to a library function, bootstrap, etc.)
- The assumptions made should be given (e.g., Normally distributed errors).

- It should be clear whether the error bar is the standard deviation or the standard error of the mean.
- It is OK to report 1-sigma error bars, but one should state it. The authors should preferably report a 2-sigma error bar than state that they have a 96% CI, if the hypothesis of Normality of errors is not verified.
- For asymmetric distributions, the authors should be careful not to show in tables or figures symmetric error bars that would yield results that are out of range (e.g. negative error rates).
- If error bars are reported in tables or plots, The authors should explain in the text how they were calculated and reference the corresponding figures or tables in the text.

8. Experiments compute resources

Question: For each experiment, does the paper provide sufficient information on the computer resources (type of compute workers, memory, time of execution) needed to reproduce the experiments?

Answer: [\[Yes\]](#)

Justification: We provide the details of computing resources in Appendix H.

Guidelines:

- The answer NA means that the paper does not include experiments.
- The paper should indicate the type of compute workers CPU or GPU, internal cluster, or cloud provider, including relevant memory and storage.
- The paper should provide the amount of compute required for each of the individual experimental runs as well as estimate the total compute.
- The paper should disclose whether the full research project required more compute than the experiments reported in the paper (e.g., preliminary or failed experiments that didn't make it into the paper).

9. Code of ethics

Question: Does the research conducted in the paper conform, in every respect, with the NeurIPS Code of Ethics <https://neurips.cc/public/EthicsGuidelines>?

Answer: [\[Yes\]](#)

Justification: The research conducted conform the NeurIPS Code of Ethics.

Guidelines:

- The answer NA means that the authors have not reviewed the NeurIPS Code of Ethics.
- If the authors answer No, they should explain the special circumstances that require a deviation from the Code of Ethics.
- The authors should make sure to preserve anonymity (e.g., if there is a special consideration due to laws or regulations in their jurisdiction).

10. Broader impacts

Question: Does the paper discuss both potential positive societal impacts and negative societal impacts of the work performed?

Answer: [\[No\]](#)

Justification: This work is not yet ready for real applications, so it has little societal impacts.

Guidelines:

- The answer NA means that there is no societal impact of the work performed.
- If the authors answer NA or No, they should explain why their work has no societal impact or why the paper does not address societal impact.
- Examples of negative societal impacts include potential malicious or unintended uses (e.g., disinformation, generating fake profiles, surveillance), fairness considerations (e.g., deployment of technologies that could make decisions that unfairly impact specific groups), privacy considerations, and security considerations.

- The conference expects that many papers will be foundational research and not tied to particular applications, let alone deployments. However, if there is a direct path to any negative applications, the authors should point it out. For example, it is legitimate to point out that an improvement in the quality of generative models could be used to generate deepfakes for disinformation. On the other hand, it is not needed to point out that a generic algorithm for optimizing neural networks could enable people to train models that generate Deepfakes faster.
- The authors should consider possible harms that could arise when the technology is being used as intended and functioning correctly, harms that could arise when the technology is being used as intended but gives incorrect results, and harms following from (intentional or unintentional) misuse of the technology.
- If there are negative societal impacts, the authors could also discuss possible mitigation strategies (e.g., gated release of models, providing defenses in addition to attacks, mechanisms for monitoring misuse, mechanisms to monitor how a system learns from feedback over time, improving the efficiency and accessibility of ML).

11. Safeguards

Question: Does the paper describe safeguards that have been put in place for responsible release of data or models that have a high risk for misuse (e.g., pretrained language models, image generators, or scraped datasets)?

Answer: **[No]**

Justification: We do not have data or models that have a high risk for misuse.

Guidelines:

- The answer NA means that the paper poses no such risks.
- Released models that have a high risk for misuse or dual-use should be released with necessary safeguards to allow for controlled use of the model, for example by requiring that users adhere to usage guidelines or restrictions to access the model or implementing safety filters.
- Datasets that have been scraped from the Internet could pose safety risks. The authors should describe how they avoided releasing unsafe images.
- We recognize that providing effective safeguards is challenging, and many papers do not require this, but we encourage authors to take this into account and make a best faith effort.

12. Licenses for existing assets

Question: Are the creators or original owners of assets (e.g., code, data, models), used in the paper, properly credited and are the license and terms of use explicitly mentioned and properly respected?

Answer: **[Yes]**

Justification: The assets are properly credited, and the license and terms of use can be found in the references.

Guidelines:

- The answer NA means that the paper does not use existing assets.
- The authors should cite the original paper that produced the code package or dataset.
- The authors should state which version of the asset is used and, if possible, include a URL.
- The name of the license (e.g., CC-BY 4.0) should be included for each asset.
- For scraped data from a particular source (e.g., website), the copyright and terms of service of that source should be provided.
- If assets are released, the license, copyright information, and terms of use in the package should be provided. For popular datasets, paperswithcode.com/datasets has curated licenses for some datasets. Their licensing guide can help determine the license of a dataset.
- For existing datasets that are re-packaged, both the original license and the license of the derived asset (if it has changed) should be provided.

- If this information is not available online, the authors are encouraged to reach out to the asset's creators.

13. New assets

Question: Are new assets introduced in the paper well documented and is the documentation provided alongside the assets?

Answer: [No]

Justification: We will release new assets in the future.

Guidelines:

- The answer NA means that the paper does not release new assets.
- Researchers should communicate the details of the dataset/code/model as part of their submissions via structured templates. This includes details about training, license, limitations, etc.
- The paper should discuss whether and how consent was obtained from people whose asset is used.
- At submission time, remember to anonymize your assets (if applicable). You can either create an anonymized URL or include an anonymized zip file.

14. Crowdsourcing and research with human subjects

Question: For crowdsourcing experiments and research with human subjects, does the paper include the full text of instructions given to participants and screenshots, if applicable, as well as details about compensation (if any)?

Answer: [NA]

Justification: We do not include experiments with human subjects.

Guidelines:

- The answer NA means that the paper does not involve crowdsourcing nor research with human subjects.
- Including this information in the supplemental material is fine, but if the main contribution of the paper involves human subjects, then as much detail as possible should be included in the main paper.
- According to the NeurIPS Code of Ethics, workers involved in data collection, curation, or other labor should be paid at least the minimum wage in the country of the data collector.

15. Institutional review board (IRB) approvals or equivalent for research with human subjects

Question: Does the paper describe potential risks incurred by study participants, whether such risks were disclosed to the subjects, and whether Institutional Review Board (IRB) approvals (or an equivalent approval/review based on the requirements of your country or institution) were obtained?

Answer: [NA]

Justification: We do not include participant study.

Guidelines:

- The answer NA means that the paper does not involve crowdsourcing nor research with human subjects.
- Depending on the country in which research is conducted, IRB approval (or equivalent) may be required for any human subjects research. If you obtained IRB approval, you should clearly state this in the paper.
- We recognize that the procedures for this may vary significantly between institutions and locations, and we expect authors to adhere to the NeurIPS Code of Ethics and the guidelines for their institution.
- For initial submissions, do not include any information that would break anonymity (if applicable), such as the institution conducting the review.

16. Declaration of LLM usage

Question: Does the paper describe the usage of LLMs if it is an important, original, or non-standard component of the core methods in this research? Note that if the LLM is used only for writing, editing, or formatting purposes and does not impact the core methodology, scientific rigorousness, or originality of the research, declaration is not required.

Answer: [NA]

Justification: We do not use LLMs in this work.

Guidelines:

- The answer NA means that the core method development in this research does not involve LLMs as any important, original, or non-standard components.
- Please refer to our LLM policy (<https://neurips.cc/Conferences/2025/LLM>) for what should or should not be described.

Appendices

A Proofs

Proposition 1. When

$$\mathcal{L}_{\text{Diff}}(\theta) = \mathbb{E}_{\mathbf{x}_0, \mathbf{z}, t} \|\mathbf{v}_\theta(\mathbf{x}_t, t) - (\alpha'_t \mathbf{x}_0 + \sigma'_t \mathbf{z})\|_2^2$$

reaches its minimum, the optimal solution $\mathbf{v}_\theta^*(\mathbf{x}_t, t)$ is

$$\mathbf{v}(\mathbf{x}_t, t) = \mathbb{E}_{\mathbf{x}_0, \mathbf{z}} (\alpha'_t \mathbf{x}_0 + \sigma'_t \mathbf{z} | \mathbf{x}_t).$$

Proof. Since

$$\begin{aligned} \mathcal{L}_{\text{Diff}}(\theta) &= \mathbb{E}_{\mathbf{x}_0, \mathbf{z}, t} \|\mathbf{v}_\theta(\mathbf{x}_t, t) - (\alpha'_t \mathbf{x}_0 + \sigma'_t \mathbf{z})\|_2^2 \\ &= \mathbb{E}_{\mathbf{x}_t, t} \mathbb{E}_{\mathbf{x}_0, \mathbf{z}} [\|\mathbf{v}_\theta(\mathbf{x}_t, t) - (\alpha'_t \mathbf{x}_0 + \sigma'_t \mathbf{z})\|_2^2 | \mathbf{x}_t] \\ &= \mathbb{E}_{\mathbf{x}_t, t} [\mathbb{E}_{\mathbf{x}_0, \mathbf{z}} [\|\mathbf{v}_\theta(\mathbf{x}_t, t)\|_2^2 | \mathbf{x}_t] - 2\mathbb{E}_{\mathbf{x}_0, \mathbf{z}} [\langle \mathbf{v}_\theta(\mathbf{x}_t, t), \alpha'_t \mathbf{x}_0 + \sigma'_t \mathbf{z} \rangle | \mathbf{x}_t] \\ &\quad + \mathbb{E}_{\mathbf{x}_0, \mathbf{z}} [\|\alpha'_t \mathbf{x}_0 + \sigma'_t \mathbf{z}\|_2^2 | \mathbf{x}_t]] \\ &= \mathbb{E}_{\mathbf{x}_t, t} (\|\mathbf{v}_\theta(\mathbf{x}_t, t)\|_2^2 - 2\mathbb{E}_{\mathbf{x}_0, \mathbf{z}} [\langle \mathbf{v}_\theta(\mathbf{x}_t, t), \alpha'_t \mathbf{x}_0 + \sigma'_t \mathbf{z} \rangle | \mathbf{x}_t] \\ &\quad + \mathbb{E}_{\mathbf{x}_0, \mathbf{z}} [\|\alpha'_t \mathbf{x}_0 + \sigma'_t \mathbf{z}\|_2^2 | \mathbf{x}_t]) \\ &= \mathbb{E}_{\mathbf{x}_t, t} (\|\mathbf{v}_\theta(\mathbf{x}_t, t)\|_2^2 - 2\langle \mathbf{v}_\theta(\mathbf{x}_t, t), \mathbb{E}_{\mathbf{x}_0, \mathbf{z}} [\alpha'_t \mathbf{x}_0 + \sigma'_t \mathbf{z} | \mathbf{x}_t] \rangle \\ &\quad + \mathbb{E}_{\mathbf{x}_0, \mathbf{z}} [\|\alpha'_t \mathbf{x}_0 + \sigma'_t \mathbf{z}\|_2^2 | \mathbf{x}_t]) \\ &= \mathbb{E}_{\mathbf{x}_t, t} (\|\mathbf{v}_\theta(\mathbf{x}_t, t)\|_2^2 - 2\langle \mathbf{v}_\theta(\mathbf{x}_t, t), \mathbf{v}(\mathbf{x}_t, t) \rangle + \|\mathbf{v}(\mathbf{x}_t, t)\|_2^2 \\ &\quad - \|\mathbf{v}(\mathbf{x}_t, t)\|_2^2 + \mathbb{E}_{\mathbf{x}_0, \mathbf{z}} [\|\alpha'_t \mathbf{x}_0 + \sigma'_t \mathbf{z}\|_2^2 | \mathbf{x}_t]) \\ &= \mathbb{E}_{\mathbf{x}_t, t} (\|\mathbf{v}_\theta(\mathbf{x}_t, t) - \mathbf{v}(\mathbf{x}_t, t)\|_2^2 - \|\mathbf{v}(\mathbf{x}_t, t)\|_2^2 + \mathbb{E}_{\mathbf{x}_0, \mathbf{z}} [\|\alpha'_t \mathbf{x}_0 + \sigma'_t \mathbf{z}\|_2^2 | \mathbf{x}_t]), \end{aligned}$$

we have the optimal solution $\mathbf{v}_\theta^*(\mathbf{x}_t, t) = \mathbf{v}(\mathbf{x}_t, t)$. \square

The above is a basic result in literature of diffusion models [66]. We prove it here since it has close relation to the following theorems.

Theorem 2 (SDEI). Let $\mathbf{f}_\theta(\mathbf{x}_t, t, s)$ be a neural network, and $\mathbf{v}(\mathbf{x}_t, t) = \mathbb{E}(\alpha'_t \mathbf{x}_0 + \sigma'_t \mathbf{z} | \mathbf{x}_t)$. Assume $\mathbf{v}(\mathbf{x}_t, t)$ is L -Lipschitz continuous in its first argument, i.e., $\|\mathbf{v}(\mathbf{x}_1, t) - \mathbf{v}(\mathbf{x}_2, t)\|_2 \leq L \|\mathbf{x}_1 - \mathbf{x}_2\|_2$ for all $\mathbf{x}_1, \mathbf{x}_2 \in \mathbb{R}^n$, $t \in [0, 1]$. Then, for each fixed t , in a sufficient small neighborhood $|s - t| \leq h$ for some $h > 0$, if $\mathcal{L}_{\text{SDEI}}(\theta)$ reaches its minimum, we have $\mathbf{f}_\theta(\mathbf{x}_t, t, s) = \mathbf{f}(\mathbf{x}_t, t, s)$.

Proof. We prove it in two steps.

First, we show that the following loss function

$$\mathcal{L}_*(\theta) := \mathbb{E}_{\mathbf{x}_0, \mathbf{x}_1, s, t} \|\mathbf{f}_\theta(\mathbf{x}_t, t, s) - \frac{1}{s-t} \int_t^s \mathbf{v}(\mathbf{x}_t + (r-t)\mathbf{f}_{\theta-}(\mathbf{x}_t, t, r), r) dr\|_2^2 \quad (21)$$

has the same derivative with respect to θ as $\mathcal{L}_{\text{SDEI}}(\theta)$.

Let $\hat{\mathbf{x}}_r = \mathbf{x}_t + (r-t)\mathbf{f}_{\theta-}(\mathbf{x}_t, t, r)$, it follows since

$$\begin{aligned} \nabla_\theta \mathcal{L}_{\text{SDEI}}(\theta) &= \nabla_\theta \mathbb{E}_{\mathbf{x}_0, \mathbf{z}, t, s} \int_t^s \|\mathbf{f}_\theta(\mathbf{x}_t, t, s) - \mathbf{v}(\hat{\mathbf{x}}_r, r)\|_2^2 dr \\ &= \nabla_\theta \mathbb{E}_{\mathbf{x}_0, \mathbf{z}, t, s} \int_t^s (\|\mathbf{f}_\theta(\mathbf{x}_t, t, s)\|_2^2 - 2\langle \mathbf{f}_\theta(\mathbf{x}_t, t, s), \mathbf{v}(\hat{\mathbf{x}}_r, r) \rangle + \|\mathbf{v}(\hat{\mathbf{x}}_r, r)\|_2^2) dr \\ &= \nabla_\theta \mathbb{E}_{\mathbf{x}_0, \mathbf{z}, t, s} \left((s-t) \|\mathbf{f}_\theta(\mathbf{x}_t, t, s)\|_2^2 - 2\langle \mathbf{f}(\mathbf{x}_t, t, s), \int_t^s \mathbf{v}(\hat{\mathbf{x}}_r, r) dr \rangle \right. \\ &\quad \left. + \int_t^s \|\mathbf{v}(\hat{\mathbf{x}}_r, r)\|_2^2 dr \right) \\ &= \nabla_\theta \mathbb{E}_{\mathbf{x}_0, \mathbf{z}, t, s} (s-t) \|\mathbf{f}_\theta(\mathbf{x}_t, t, s) - \frac{1}{s-t} \int_t^s \mathbf{v}(\hat{\mathbf{x}}_r, r) dr\|_2^2. \end{aligned}$$

Second, we show that $\mathcal{L}_*(\theta) = \mathbf{0}$ implies $\mathbf{f}_\theta(\mathbf{x}_t, t, s) = \mathbf{f}(\mathbf{x}_t, t, s)$ in each sufficient small neighborhood of t . Using Picard iteration, we construct a sequence \mathbf{f}_n satisfying $\mathbf{f}_0 = \mathbf{0}$, $\mathbf{f}_{n+1} = \frac{1}{s-t} \int_t^s \mathbf{v}(\mathbf{x}_t + (r-t)\mathbf{f}_n(\mathbf{x}_t, t, r), r) dr$. Without loss of generality, we may assume $h > 0$. We have

$$\begin{aligned}
& \sup_{s \in (t, t+h]} \|\mathbf{f}_{n+1}(\mathbf{x}_t, t, s) - \mathbf{f}(\mathbf{x}_t, t, s)\|_2^2 \\
&= \sup_{s \in (t, t+h]} \frac{1}{(s-t)^2} \left\| \int_t^s \mathbf{v}(\mathbf{x}_t + (r-t)\mathbf{f}_n(\mathbf{x}_t, t, r), r) dr \right. \\
&\quad \left. - \int_t^s \mathbf{v}(\mathbf{x}_t + (r-t)\mathbf{f}(\mathbf{x}_t, t, r), r) dr \right\|_2^2 \\
&\leq L \sup_{s \in (t, t+h]} \frac{1}{(s-t)^2} \left\| \int_t^s (r-t)(\mathbf{f}_n(\mathbf{x}_t, t, r) - \mathbf{f}(\mathbf{x}_t, t, r)) dr \right\|_2^2 \\
&\leq L \sup_{s \in (t, t+h]} \frac{1}{(s-t)^2} \int_t^s (r-t)^2 dr \sup_{r \in [t, t+h]} \|\mathbf{f}_n(\mathbf{x}_t, t, r) - \mathbf{f}(\mathbf{x}_t, t, r)\|_2^2 \\
&= \frac{1}{3} L h \sup_{s \in (t, t+h]} \|\mathbf{f}_n(\mathbf{x}_t, t, s) - \mathbf{f}(\mathbf{x}_t, t, s)\|_2^2.
\end{aligned}$$

When $s = t$, we also have

$$\|\mathbf{f}_{n+1}(\mathbf{x}_t, t, s) - \mathbf{f}(\mathbf{x}_t, t, s)\|_2^2 = \frac{1}{3} L h \|\mathbf{f}_n(\mathbf{x}_t, t, s) - \mathbf{f}(\mathbf{x}_t, t, s)\|_2^2.$$

Therefore, $\sup_{s \in [t, t+h]} \|\mathbf{f}_{n+1}(\mathbf{x}_t, t, s) - \mathbf{f}(\mathbf{x}_t, t, s)\|_2^2$ converges to 0 when $\frac{1}{3} L h < 1$, i.e., $h < \frac{3}{L}$. This means we find a neighborhood $[t, t+h]$ for each t , such that when $\mathcal{L}_{\text{SDEI}}(\theta)$ reaches its minimum, we have $\mathbf{f}_\theta(\mathbf{x}_t, t, s) = \mathbf{f}(\mathbf{x}_t, t, s)$. \square

Theorem 3 (STEE). Let $\mathbf{f}_\theta(\mathbf{x}_t, t, s)$ be a neural network, and $\mathbf{v}(\mathbf{x}_t, t) = \mathbb{E}(\alpha'_t \mathbf{x}_0 + \sigma'_t \mathbf{z} | \mathbf{x}_t)$. Assume $\mathbf{f}_\theta(\mathbf{x}_t, t, s)$ is L -Lipschitz continuous in its first argument, i.e., $\|\mathbf{f}_\theta(\mathbf{x}_1, t, s) - \mathbf{f}_\theta(\mathbf{x}_2, t, s)\|_2 \leq L \|\mathbf{x}_1 - \mathbf{x}_2\|_2$ for all $\mathbf{x}_1, \mathbf{x}_2 \in \mathbb{R}^n$, $t, s \in [0, 1]$. Then, for each fixed $[a, b] \subseteq [0, 1]$ with $b - a$ sufficiently small, if $\mathcal{L}_{\text{STEE}}(\theta)$ reaches its minimum, we have $\mathbf{f}_\theta(\mathbf{x}_t, t, s) = \mathbf{f}(\mathbf{x}_t, t, s)$ for any $[t, s] \subseteq [a, b]$.

Proof. First, we show that $\mathcal{L}_{\text{STEE}}(\theta)$ have the same derivative with respect to θ as the following loss function

$$\mathcal{L}_*(\theta) := \mathbb{E}_{\mathbf{x}_r, s, t, r \sim \mathcal{U}(s, t)} \|\mathbf{f}_\theta(\mathbf{x}_r + (t-r)\mathbf{f}_{\theta-}(\mathbf{x}_r, r, t), t, s) - \mathbf{v}(\mathbf{x}_r, r)\|_2^2. \quad (22)$$

It follows since

$$\begin{aligned}
\nabla_\theta \mathcal{L}_{\text{STEE}}(\theta) &= \nabla_\theta \mathbb{E}_{\mathbf{x}_0, \mathbf{z}, t, s} \int_t^s \|\mathbf{f}_\theta(\mathbf{x}_r + (t-r)\mathbf{f}_{\theta-}(\mathbf{x}_r, r, t), t, s) - (\alpha'_r \mathbf{x}_0 + \sigma'_r \mathbf{z})\|_2^2 dr \\
&= \nabla_\theta \mathbb{E}_{\mathbf{x}_r, t, s} \mathbb{E}_{\mathbf{x}_0, \mathbf{z}} \int_t^s [\|\mathbf{f}_\theta(\mathbf{x}_r + (t-r)\mathbf{f}_{\theta-}(\mathbf{x}_r, r, t), t, s) - \alpha'_r \mathbf{x}_0 + \sigma'_r \mathbf{z}\|_2^2 | \mathbf{x}_r] dr \\
&= \nabla_\theta \mathbb{E}_{\mathbf{x}_r, t, s} \int_t^s (\mathbb{E}_{\mathbf{x}_0, \mathbf{z}} [\|\mathbf{f}_\theta(\mathbf{x}_r + (t-r)\mathbf{f}_{\theta-}(\mathbf{x}_r, r, t), t, s)\|_2^2 | \mathbf{x}_r] \\
&\quad - 2 \mathbb{E}_{\mathbf{x}_0, \mathbf{z}} [\langle \mathbf{f}_\theta(\mathbf{x}_r + (t-r)\mathbf{f}_{\theta-}(\mathbf{x}_r, r, t), t, s), \alpha'_r \mathbf{x}_0 + \sigma'_r \mathbf{z} \rangle | \mathbf{x}_r] \\
&\quad + \mathbb{E}_{\mathbf{x}_0, \mathbf{z}} [\|\alpha'_r \mathbf{x}_0 + \sigma'_r \mathbf{z}\|_2^2 | \mathbf{x}_r]) dr \\
&= \nabla_\theta \mathbb{E}_{\mathbf{x}_r, t, s} \int_t^s \|\mathbf{f}_\theta(\mathbf{x}_r + (t-r)\mathbf{f}_{\theta-}(\mathbf{x}_r, r, t), t, s)\|_2^2 dr \\
&\quad - 2 \int_t^s \langle \mathbf{f}_\theta(\mathbf{x}_r + (t-r)\mathbf{f}_{\theta-}(\mathbf{x}_r, r, t), t, s), \mathbb{E}_{\mathbf{x}_0, \mathbf{z}} [\alpha'_r \mathbf{x}_0 + \sigma'_r \mathbf{z} | \mathbf{x}_r] \rangle dr \\
&\quad + \int_t^s \mathbb{E}_{\mathbf{x}_0, \mathbf{z}} [\|\alpha'_r \mathbf{x}_0 + \sigma'_r \mathbf{z}\|_2^2 | \mathbf{x}_r] dr
\end{aligned}$$

$$= \nabla_{\theta} \mathbb{E}_{\mathbf{x}_r, t, s} \int_t^s \|\mathbf{f}_{\theta}(\mathbf{x}_r + (t-r)\mathbf{f}_{\theta-}(\mathbf{x}_r, r, t), t, s) - \mathbf{v}(\mathbf{x}_r, r)\|_2^2 dr.$$

Then, notice that when $\mathcal{L}_*(\theta)$ achieves its minimum, we have

$$\mathcal{L}_{**}(\theta) := \left\| \int_t^s \mathbf{f}_{\theta}(\mathbf{x}_r + (t-r)\mathbf{f}_{\theta-}(\mathbf{x}_r, r, t), t, s) dr - \int_t^s \mathbf{v}(\mathbf{x}_r, r) dr \right\|_2^2 = 0. \quad (23)$$

If not, denote $\mathbf{g}_{\theta}(\mathbf{x}_r, r, t, s) = \mathbf{f}_{\theta}(\mathbf{x}_r + (t-r)\mathbf{f}_{\theta-}(\mathbf{x}_r, r, t), t, s)$, and assume $\mathcal{L}_*(\theta)$ reaches the minimum without $\int_t^s \mathbf{g}_{\theta}(\mathbf{x}_r, r, t, s) dr = \int_t^s \mathbf{v}(\mathbf{x}_r, r) dr$.

Let $\tilde{\mathbf{g}}_{\theta}(\mathbf{x}_r, r, t, s) = \mathbf{g}_{\theta}(\mathbf{x}_r, r, t, s) + \frac{1}{s-t} \int_t^s \mathbf{v}(\mathbf{x}_r, r) dr - \frac{1}{s-t} \int_t^s \mathbf{g}_{\theta}(\mathbf{x}_r, r, t, s) dr$, then we have

$$\begin{aligned} & \int_t^s \|\tilde{\mathbf{g}}_{\theta}(\mathbf{x}_r, r, t, s) - \mathbf{v}(\mathbf{x}_r, r)\|_2^2 dr \\ &= \int_t^s \|\mathbf{g}_{\theta}(\mathbf{x}_r, r, t, s) - \mathbf{v}(\mathbf{x}_r, r) + \frac{1}{s-t} \int_t^s \mathbf{v}(\mathbf{x}_r, r) dr - \frac{1}{s-t} \int_t^s \mathbf{g}_{\theta}(\mathbf{x}_r, r, t, s) dr\|_2^2 \\ &= \int_t^s \|\mathbf{g}_{\theta}(\mathbf{x}_r, r, t, s) - \mathbf{v}(\mathbf{x}_r, r)\|_2^2 dr \\ & \quad + \int_t^s \left\| \frac{1}{s-t} \int_t^s \mathbf{v}(\mathbf{x}_r, r) dr - \frac{1}{s-t} \int_t^s \mathbf{g}_{\theta}(\mathbf{x}_r, r, t, s) dr \right\|_2^2 \\ & \quad + 2 \int_t^s \langle \mathbf{g}_{\theta}(\mathbf{x}_r, r, t, s) - \mathbf{v}(\mathbf{x}_r, r), \frac{1}{s-t} \int_t^s \mathbf{v}(\mathbf{x}_r, r) dr - \frac{1}{s-t} \int_t^s \mathbf{g}_{\theta}(\mathbf{x}_r, r, t, s) dr \rangle dr \\ &= \int_t^s \|\mathbf{g}_{\theta}(\mathbf{x}_r, r, t, s) - \mathbf{v}(\mathbf{x}_r, r)\|_2^2 dr \\ & \quad + (s-t) \left\| \frac{1}{s-t} \int_t^s \mathbf{v}(\mathbf{x}_r, r) dr - \frac{1}{s-t} \int_t^s \mathbf{g}_{\theta}(\mathbf{x}_r, r, t, s) dr \right\|_2^2 \\ & \quad + 2 \left\langle \int_t^s (\mathbf{g}_{\theta}(\mathbf{x}_r, r, t, s) - \mathbf{v}(\mathbf{x}_r, r)) dr, \frac{1}{s-t} \int_t^s \mathbf{v}(\mathbf{x}_r, r) dr - \frac{1}{s-t} \int_t^s \mathbf{g}_{\theta}(\mathbf{x}_r, r, t, s) dr \right\rangle \\ &= \int_t^s \|\mathbf{g}_{\theta}(\mathbf{x}_r, r, t, s) - \mathbf{v}(\mathbf{x}_r, r)\|_2^2 dr \\ & \quad - (s-t) \left\| \frac{1}{s-t} \int_t^s \mathbf{v}(\mathbf{x}_r, r) dr - \frac{1}{s-t} \int_t^s \mathbf{g}_{\theta}(\mathbf{x}_r, r, t, s) dr \right\|_2^2 \\ &< \int_t^s \|\mathbf{g}_{\theta}(\mathbf{x}_r, r, t, s) - \mathbf{v}(\mathbf{x}_r, r)\|_2^2 dr, \end{aligned}$$

which is a contradictory.

Next, we prove that minimizing $\mathcal{L}_{**}(\theta)$ implies $\mathbf{f}_{\theta}(\mathbf{x}_t, t, s) = \mathbf{f}(\mathbf{x}_t, t, s)$ for all $[t, s] \subseteq [a, b] \subseteq [0, 1]$, where $b - a$ is sufficiently small.

Using Picard iteration, we construct a sequence \mathbf{f}_n satisfying $\mathbf{f}_0 = \mathbf{0}$, $\mathbf{f}_{n+1}(\mathbf{x}_r + (t-r)\mathbf{f}_n(\mathbf{x}_r, r, t), t, s) = \mathbf{f}(\mathbf{x}_t, t, s)$.

When $s \neq t$, we have

$$\begin{aligned} & \sup_{t, s \in [a, b]} \|\mathbf{f}_{n+1}(\mathbf{x}_t, t, s) - \mathbf{f}(\mathbf{x}_t, t, s)\|_2^2 \\ &= \sup_{t, s \in [a, b]} \frac{1}{s-t} \int_t^s \|\mathbf{f}_{n+1}(\mathbf{x}_t, t, s) - \mathbf{f}(\mathbf{x}_t, t, s)\|_2^2 dr \\ &\leq \sup_{t, s \in [a, b]} \frac{1}{s-t} \int_t^s \|\mathbf{f}_{n+1}(\mathbf{x}_t, t, s) - \mathbf{f}_{n+1}(\mathbf{x}_r + (t-r)\mathbf{f}_n(\mathbf{x}_r, r, t), t, s)\|_2^2 dr \\ &\leq L \sup_{t, s \in [a, b]} \frac{1}{s-t} \int_t^s \|\mathbf{x}_t - \mathbf{x}_r - (t-r)\mathbf{f}_n(\mathbf{x}_r, r, t)\|_2^2 dr \\ &= L \sup_{t, s \in [a, b]} \frac{1}{s-t} \int_t^s \|\mathbf{x}_r + (t-r)\mathbf{f}_n(\mathbf{x}_r, r, t) - \mathbf{x}_r - (t-r)\mathbf{f}(\mathbf{x}_r, r, t)\|_2^2 dr \end{aligned}$$

$$\begin{aligned}
&\leq L \sup_{t,s \in [a,b]} \frac{1}{s-t} \int_t^s |t-r|^2 dr \sup_{r,s \in [a,b]} \|\mathbf{f}_n(\mathbf{x}_r, r, t) - \mathbf{f}(\mathbf{x}_r, r, t)\|_2^2 \\
&= L \sup_{t,s \in [a,b]} \frac{(s-t)^2}{3} \sup_{r,s \in [a,b]} \|\mathbf{f}_n(\mathbf{x}_r, r, t) - \mathbf{f}(\mathbf{x}_r, r, t)\|_2^2 \\
&\leq \frac{1}{3} L(b-a)^2 \sup_{t,s \in [a,b]} \|\mathbf{f}_n(\mathbf{x}_t, t, s) - \mathbf{f}(\mathbf{x}_t, t, s)\|_2^2.
\end{aligned}$$

Also when $s = t$, the inequality satisfies.

One can see with sufficiently small $b - a$, $\sup_{t,s \in [a,b]} \|\mathbf{f}_{n+1}(\mathbf{x}_t, t, s) - \mathbf{f}(\mathbf{x}_t, t, s)\|_2^2$ converges to 0. Hence, there exists a small interval, such that when $\mathcal{L}_{\text{STEE}}(\theta)$ reaches the minimum, we have $\mathbf{f}_\theta(\mathbf{x}_t, t, s) = \mathbf{f}(\mathbf{x}_t, t, s)$.

□

Corollary 5 (STEI). *Let $\mathbf{f}_\theta(\mathbf{x}_t, t, s)$ be a neural network, and let $\mathbf{v}(\mathbf{x}_t, t)$ be the true velocity field. Assume $\mathbf{v}(\mathbf{x}_t, t)$ is L -Lipschitz continuous in its first argument. If $\mathcal{L}_{\text{STEI}}(\theta)$ reaches its minimum, then for any interval where $|s - t| \leq h$ and $h < \frac{3}{L}$, we have $\mathbf{f}_\theta(\mathbf{x}_t, t, s) = \mathbf{f}(\mathbf{x}_t, t, s)$.*

Proof. The loss $\mathcal{L}_{\text{STEI}}(\theta)$ is defined as a sum of a secant term and a diffusion term

$$\mathcal{L}_{\text{STEI}}(\theta) = \mathbb{E}[\|\mathbf{f}_\theta(\mathbf{x}_t, t, s) - \mathbf{f}_{\theta-}(\hat{\mathbf{x}}_r, r, r)\|_2^2] + \lambda \mathbb{E}[\|\mathbf{f}_\theta(\mathbf{x}_\tau, \tau, \tau) - (\alpha'_\tau \mathbf{x}_0 + \sigma'_\tau \mathbf{z})\|_2^2]$$

where $\hat{\mathbf{x}}_r = \mathbf{x}_t + (r - t)\mathbf{f}_{\theta-}(\mathbf{x}_t, t, r)$. For $\mathcal{L}_{\text{STEI}}(\theta)$ to reach the minimum, both two terms must reach the minimum. By Proposition 1, the diffusion term achieves the minimum if and only if

$$\mathbf{f}_\theta(\mathbf{x}_t, t, t) = \mathbb{E}(\alpha'_t \mathbf{x}_0 + \sigma'_t \mathbf{z} | \mathbf{x}_t) = \mathbf{v}(\mathbf{x}_t, t).$$

Substituting this result into the secant term, it becomes the one studied in the proof of Theorem 2. The remainder of the proof follows identically. □

Corollary 6 (SDEE). *Let $\mathbf{f}_\theta(\mathbf{x}_t, t, s)$ be a neural network that is L -Lipschitz continuous in its first argument. For any fixed interval $[a, b] \subseteq [0, 1]$ with $b - a$ sufficiently small, if $\mathcal{L}_{\text{SDEE}}(\theta)$ reaches its minimum, then $\mathbf{f}_\theta(\mathbf{x}_t, t, s) = \mathbf{f}(\mathbf{x}_t, t, s)$.*

Proof. The SDEE loss is defined as

$$\mathcal{L}_{\text{SDEE}}(\theta) = \mathbb{E}[\|\mathbf{f}_\theta(\mathbf{x}_r + (t - r)\mathbf{f}_{\theta-}(\mathbf{x}_r, r, t), t, s) - \mathbf{v}(\mathbf{x}_r, r)\|_2^2].$$

This loss function is identical to the intermediate objective $\mathcal{L}_*(\theta)$ analyzed in the proof of Theorem 3. The proof, therefore, follows that of Theorem 3 directly. □

B Derivations

B.1 Applying to EDM

The training objective of EDM [6] is

$$\mathcal{L}_{\text{EDM}}(\theta) = \mathbb{E}_{\sigma, \mathbf{y}, \mathbf{n}} w(\sigma) \|\mathbf{F}_\theta(c_{\text{in}}(\sigma) \cdot (\mathbf{y} + \mathbf{n}), c_{\text{noise}}(\sigma)) - \frac{1}{c_{\text{out}}(\sigma)} (\mathbf{y} - c_{\text{skip}}(\sigma) \cdot (\mathbf{y} + \mathbf{n}))\|_2^2, \quad (24)$$

where \mathbf{F}_θ is the neural network, $w(\sigma)$ the loss weighting factor, $c_{\text{in}}(\sigma) = \frac{1}{\sqrt{\sigma^2 + \sigma_d^2}}$, $c_{\text{out}}(\sigma) = \frac{\sigma \cdot \sigma_d}{\sqrt{\sigma^2 + \sigma_d^2}}$, $c_{\text{skip}}(\sigma) = \frac{\sigma_d^2}{\sigma^2 + \sigma_d^2}$, $c_{\text{noise}} = \frac{1}{4} \ln(\sigma)$, and $\sigma_d = 0.5$ is the variance of the image data p_d . Since $\mathbf{y} \sim p_d$, $\mathbf{n} \sim \mathcal{N}(\mathbf{0}, \sigma^2 \mathbf{I})$, we can denote \mathbf{y} by \mathbf{x}_0 , \mathbf{n} by $\sigma \mathbf{z}$ in our notation. Then Eq. (24) can be simplified to

$$\begin{aligned}
\mathcal{L}_{\text{EDM}}(\theta) &= \mathbb{E}_{\sigma, \mathbf{x}_0, \mathbf{z}} \frac{w(\sigma)}{\sigma_d^2} \left\| -\sigma_d \mathbf{F}_\theta \left(\frac{1}{\sigma_d} \left(\frac{\sigma_d}{\sqrt{\sigma^2 + \sigma_d^2}} \mathbf{x}_0 + \frac{\sigma}{\sqrt{\sigma^2 + \sigma_d^2}} \sigma_d \mathbf{z} \right), c_{\text{noise}}(\sigma) \right) \right. \\
&\quad \left. - \left(-\frac{\sigma}{\sqrt{\sigma^2 + \sigma_d^2}} \mathbf{x}_0 + \frac{\sigma_d}{\sqrt{\sigma^2 + \sigma_d^2}} \sigma_d \mathbf{z} \right) \right\|_2^2. \quad (25)
\end{aligned}$$

The Trigflow framework [35] demonstrates that if letting $t = \arctan(\frac{\sigma}{\sigma_d})$ and $\mathbf{x}_t = \cos(t)\mathbf{x}_0 + \sin(t)\sigma_d\mathbf{z}$ where $t \in [0, \frac{\pi}{2}]$, training with the simplified objective

$$\mathcal{L}_{\text{EDM}}(\theta) = \mathbb{E}_{\mathbf{x}_0, \mathbf{z}, t} \frac{w(t)}{\sigma_d^2} \left\| -\sigma_d \mathbf{F}_\theta \left(\frac{\mathbf{x}_t}{\sigma_d}, c_{\text{noise}}(\sigma_d \cdot \tan(t)) \right) - (-\sin(t)\mathbf{x}_0 + \cos(t)\sigma_d\mathbf{z}) \right\|_2^2 \quad (26)$$

leads to the diffusion ODE

$$\frac{d\mathbf{x}_t}{dt} = -\sigma_d \mathbf{F}_\theta \left(\frac{\mathbf{x}_t}{\sigma_d}, c_{\text{noise}}(\sigma_d \cdot \tan(t)) \right). \quad (27)$$

As a result, to adapt the notions in Section 3 to the EDM loss, we can modify the range of time to $[0, \frac{\pi}{2}]$, substitute \mathbf{z} with $\sigma_d\mathbf{z}$ and let $\mathbf{v}(\mathbf{x}_t, t) = -\sigma_d \mathbf{F}_\theta \left(\frac{\mathbf{x}_t}{\sigma_d}, c_{\text{noise}}(\sigma_d \cdot \tan(t)) \right)$, $\alpha_t = \cos(t)$, $\sigma_t = \sin(t)$.

For practical choices in transferring EDM to the secant version, we simply set the loss weight $\frac{w(t)}{\sigma_d} = 1$. Besides, since $t \rightarrow 0$ or $t \rightarrow \frac{\pi}{2}$ makes $c_{\text{noise}}(\sigma_d \tan(t)) = \frac{1}{4} \ln(\sigma_d \tan(t)) \rightarrow \infty$, we constrain t and s within the range of $[0.001, \frac{\pi}{2} - 0.00625]$.

B.2 Applying to SiT

The training objective of SiT [39]⁴ is the flow matching loss

$$\mathcal{L}_{\text{FM}}(\theta) = \mathbb{E}_{\mathbf{x}_0, \mathbf{x}_1, t} \|\mathbf{v}_\theta(\mathbf{x}_t, t) - (\mathbf{x}_1 - \mathbf{x}_0)\|_2^2. \quad (28)$$

To adapt our notation to loss Eq. (28), we can substitute \mathbf{x}_0 with \mathbf{x}_1 , and \mathbf{z} with \mathbf{x}_0 , and set $\alpha_t = t$ and $\sigma_t = 1 - t$.

C Model Parametrization

C.1 The Secant Version of EDM

The parametrization is similar to that in CTM [34]. Specifically, we apply the same time embedder for the extra s input as that employed for t . In each UNet block, we add affine layers for the s embedding, which projects the s embedding into the AdaGN [5] parameters, akin to that for t embedding. The resulting AdaGN parameters from both s and t are then added up. The weights of all the added layers are randomly initialized.

C.2 The Secant Version of DiT

We clone (including the pretrained parameters) the time embedder of t as the s embedder. The original time embedding is replaced with half of the summed embeddings from t and s . This design ensures $\mathbf{f}_\theta(\mathbf{x}_t, t, t) = \mathbf{v}_\theta(\mathbf{x}_t, t)$ when loading the pretrained SiT weights. For classifier-free guidance, we add another time embedder for the CFG scale w , whose weights are randomly initialized.

We also tried the parametrization in Section C.1 for DiT, and find that the performances are comparable. However, this implementation introduces significantly more parameters ($\sim 226\text{M}$), since the module for producing AdaLN parameters is very large.

D Training Algorithms for STEI and SDEE

Similar to Algorithm 1 for $\mathcal{L}_{\text{SDEI}}$ and Algorithm 2 for $\mathcal{L}_{\text{STEE}}$, we provide the training algorithms with $\mathcal{L}_{\text{STEI}}$ and $\mathcal{L}_{\text{SDEE}}$ in Algorithm 3 and Algorithm 4, respectively.

⁴The loss configuration follows *linear path* and *velocity prediction*. Details can be found at <https://github.com/willisma/SiT>.

Algorithm 3 Secant Training by Estimating the Interior Point (STEI)

Input: dataset \mathcal{D} , neural network f_θ , learning rate η

repeat

$$\theta^- \leftarrow \theta$$

 Sample $\mathbf{x} \sim \mathcal{D}$, $\mathbf{z} \sim \mathcal{N}(\mathbf{0}, \mathbf{I})$

 Sample t and s

 Sample $r \sim \mathcal{U}[0, 1]$, $r \leftarrow t + r(s - t)$

$\mathbf{x}_t \leftarrow t\mathbf{x} + (1 - t)\mathbf{z}$

$\hat{\mathbf{x}}_r \leftarrow \mathbf{x}_t + (r - t)\mathbf{f}_{\theta^-}(\mathbf{x}_t, t, r)$

$\mathbf{v}_r \leftarrow \mathbf{v}(\hat{\mathbf{x}}_r, r)$

 Sample $\tau \in \mathcal{U}[0, 1]$

$\mathbf{x}_\tau \leftarrow \tau\mathbf{x} + (1 - \tau)\mathbf{z}$

$\mathbf{u}_\tau \leftarrow \mathbf{x} - \mathbf{z}$

$\mathcal{L}(\theta) = \mathbb{E}_{\mathbf{x}, \mathbf{z}, t, s, r} \|\mathbf{f}_\theta(\mathbf{x}_t, t, s) - \mathbf{f}_\theta(\mathbf{x}_r, r, r)\|_2^2$

$+ \lambda \mathbb{E}_{\mathbf{x}_0, \mathbf{z}, \tau} \|\mathbf{f}_\theta(\mathbf{x}_\tau, \tau, \tau) - \mathbf{u}_\tau\|_2^2$

$\theta \leftarrow \theta - \eta \nabla_\theta \mathcal{L}(\theta)$

until convergence

Algorithm 4 Secant Distillation by Estimating the End Point (SDEE)

Input: dataset \mathcal{D} , neural network f_θ , teacher diffusion model v , learning rate η

repeat

$$\theta^- \leftarrow \theta$$

 Sample $\mathbf{x} \sim \mathcal{D}$, $\mathbf{z} \sim \mathcal{N}(\mathbf{0}, \mathbf{I})$

 Sample t and $s \sim \mathcal{U}[0, 1]$

 Sample $r \sim \mathcal{U}[0, 1]$, $r \leftarrow t + r(s - t)$

$\mathbf{x}_r \leftarrow r\mathbf{x} + (1 - r)\mathbf{z}$

$\hat{\mathbf{x}}_t \leftarrow \mathbf{x}_r + (t - r)\mathbf{f}_{\theta^-}(\mathbf{x}_r, r, t)$

$\mathcal{L}(\theta) = \mathbb{E}_{\mathbf{x}, \mathbf{z}, t, s, r} \|\mathbf{f}_\theta(\hat{\mathbf{x}}_t, t, s) - \mathbf{v}(\mathbf{x}_r, r)\|_2^2$

$\theta \leftarrow \theta - \eta \nabla_\theta \mathcal{L}(\theta)$

until convergence

Algorithm 5 Sampling of t, s in SDEI and STEI for EDM

Input: Gaussian distribution parameter P_{mean} and P_{std} , number of steps N , boundary constants ϵ_1 and ϵ_2

Output: sampled time point t and s

Sample $\sigma \sim \mathcal{N}(P_{\text{mean}}, P_{\text{std}})$

$t \leftarrow \arctan\left(\frac{\sigma}{\sigma_d}\right)$

Clip t into $[\epsilon_1, \frac{\pi}{2} - \epsilon_2]$

Round t to be discrete

Sample $d \sim \mathcal{U}(0, \frac{1}{N})$

$s \leftarrow t - d$

Clip s into $[\epsilon_1, \frac{\pi}{2} - \epsilon_2]$

Algorithm 6 Sampling of t, s in SDEE and STEE for EDM

Input: Gaussian distribution parameter P_{mean} and P_{std} , number of steps N , boundary constants ϵ_1 and ϵ_2

Output: sampled time point t and s

Sample $\sigma \sim \mathcal{N}(P_{\text{mean}}, P_{\text{std}})$

$t \leftarrow \arctan\left(\frac{\sigma}{\sigma_d}\right)$

Clip t into $[\epsilon_1, \frac{\pi}{2} - \epsilon_2]$

Sample $d \sim \mathcal{U}(0, \frac{1}{N})$

$d \leftarrow -d$ with probability of 0.5

$s \leftarrow t - d$

Clip s into $[\epsilon_1, \frac{\pi}{2} - \epsilon_2]$

Algorithm 7 Sampling of t, s in SDEI and STEI for DiT

Input: number of steps N

Output: sampled time point t and s

Sample $d \sim \mathcal{U}(0, \frac{1}{N})$

Sample $t \sim \mathcal{U}(0, 1 - d)$

Round t to be discrete (SDEI only)

$s \leftarrow t + d$

Algorithm 8 Sampling of t, s in SDEE and STEE for DiT

Input: number of steps N

Output: sampled time point t and s

Sample $d \sim \mathcal{U}(0, \frac{1}{N})$

Sample $t \sim \mathcal{U}(0, 1 - d)$

$s \leftarrow t + d$

Swap t and s with probability of 0.5

E Sampling Time Points During Training

Sampling t and s for EDM. We sample σ from the Gaussian proposal distribution with $P_{\text{mean}} = -1.0$ and $P_{\text{std}} = 1.4$ [35], which we find slightly better than the default configuration of $P_{\text{mean}} = -1.2$ and $P_{\text{std}} = 1.2$ in EDM [6], and derive t by $t = \arctan(\frac{\sigma}{\sigma_d})$. Then, we sample the distance $d = |s - t|$ by $d \sim \mathcal{U}(0, \frac{1}{N})$, where N is the pre-set number of steps. If the loss estimates the interior point, we round the sampled t to be discrete; while for losses that estimate the end point, we randomly multiply -1 to d with a probability of 0.5. Finally, we get s by $s = t - d$. The sampling processes are illustrated in Algorithm 5 and Algorithm 6.

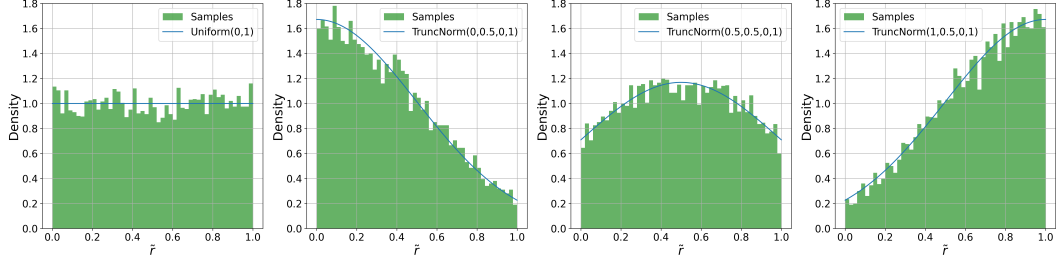


Figure 7: Uniform distribution and truncated normal distribution under different μ values.

Sampling t and s for DiT. We first sample the distance $d = |s - t|$ by $d \sim \mathcal{U}(0, \frac{1}{N})$. Then, we sample t by $t \sim \mathcal{U}(0, 1 - d)$. If estimating the interior point, we round t to be discrete and derive s by $s = t + d$; if estimating the end point, we get s by $s = t + d$ and randomly swap t and s with a probability of 0.5. The sampling strategies are illustrated in Algorithm 7 and Algorithm 8.

Sampling r . The default sampling strategy for r follows a uniform distribution between the endpoints t and s . Specifically, we first draw $\tilde{r} \sim \mathcal{U}(0, 1)$ from a standard uniform distribution, then obtain r through the linear transformation $r = t + \tilde{r}(s - t)$.

In our ablation studies, we explore alternative sampling strategies using the truncated normal distribution. Specifically, we sample \tilde{r} from a truncated normal distribution $\tilde{r} \sim \mathcal{TN}(\mu, \sigma, 0, 1)$, where the distribution is confined to the interval $[0, 1]$. The value of r is then obtained through the same linear transformation $r = t + \tilde{r}(s - t)$. Let $\tilde{q}(\tilde{r})$ denote the probability density function of $\mathcal{TN}(\mu, \sigma, 0, 1)$. Assuming $s \neq t$ without loss of generality, we can derive

$$r \sim q(r) = \frac{1}{|s - t|} \tilde{q}\left(\frac{r - t}{s - t}\right). \quad (29)$$

Then Eq. (20) becomes

$$\begin{aligned} \mathbf{f}(\mathbf{x}_t, t, s) &= \mathbb{E}_{r \sim q(r)} \mathbf{v}(\mathbf{x}_r, r) \frac{p_{\mathcal{U}(t,s)}(r)}{q(r)} \\ &= \mathbb{E}_{\tilde{r} \sim \tilde{q}(\tilde{r})} \mathbf{v}(\mathbf{x}_r, r) \frac{\frac{1}{|s-t|}}{\frac{1}{|s-t|} \tilde{q}(\tilde{r})} \\ &= \mathbb{E}_{\tilde{r} \sim \tilde{q}(\tilde{r})} \mathbf{v}(\mathbf{x}_r, r) \frac{1}{\tilde{q}(\tilde{r})}. \end{aligned} \quad (30)$$

The probability distributions of \tilde{r} under different μ values are illustrated in Fig. 7.

F Sampling Algorithms at Inference

For simplicity, we always sample adjacent time steps with uniform spacing. The sampling process differs between STEE-trained models and those trained with SDEI, STEI, or SDEE, due to their distinct handling of classifier-free guidance. The detailed sampling processes are presented in Algorithm 9 and Algorithm 10.

Algorithm 9 Sampling Using Models Trained with SDEI, STEI and SDEE

Input: model \mathbf{f}_θ , number of steps N , guidance scale w
Output: sampled image \mathbf{x}_0
 Sample $\mathbf{x}_1 \sim \mathcal{N}(\mathbf{0}, \mathbf{I})$
for $i = 0$ to $N - 1$ **do**

$$\mathbf{x}_{\frac{N-i-1}{N}} \leftarrow \mathbf{x}_{\frac{N-i}{N}} - \frac{1}{N} \mathbf{f}_\theta(\mathbf{x}_{\frac{N-i}{N}}, \frac{N-i}{N}, \frac{N-i-1}{N}, w)$$

end for

Table 7: The performance comparison of secant losses on CIFAR-10 and ImageNet-256 \times 256.

Type	Steps	CIFAR-10		ImageNet-256 \times 256		
		FID \downarrow	FID \downarrow	IS \uparrow	FID (w/ CFG) \downarrow	IS (w/ CFG) \uparrow
SDEI	1	22.67	43.49	54.40	8.97	253.25
SDEI	2	5.88	20.83	93.17	4.81	257.56
SDEI	4	3.23	14.21	116.03	3.11	258.81
SDEI	8	2.27	9.14	139.69	2.46	248.36
STEI	1	36.87	38.44	56.60	7.12	241.75
STEI	2	9.21	21.10	95.77	4.41	241.99
STEI	4	4.04	10.91	135.03	2.78	269.87
STEI	8	2.59	7.64	157.03	2.36	274.72
SDEE	4	10.19	19.99	96.87	3.96	247.20
SDEE	8	3.18	9.46	136.97	2.46	258.94
STEE	4	10.55	22.82	83.87	3.02	274.00
STEE	8	3.78	12.98	110.03	2.33	274.47

Algorithm 10 Sampling Using Models Trained with STEE

Input: model f_θ , number of steps N , guidance scale w
Output: sampled image x_0
 Sample $x_1 \sim \mathcal{N}(\mathbf{0}, \mathbf{I})$
for $i = 0$ to $N - 1$ **do**
if $w > 1$ **then**

$$f_\theta(x_{\frac{N-i}{N}}, \frac{N-i}{N}, \frac{N-i-1}{N}) \leftarrow f_\theta^u(x_{\frac{N-i}{N}}, \frac{N-i}{N}, \frac{N-i-1}{N}) + w(f_\theta^c(x_{\frac{N-i}{N}}, \frac{N-i}{N}, \frac{N-i-1}{N}) - f_\theta^u(x_{\frac{N-i}{N}}, \frac{N-i}{N}, \frac{N-i-1}{N}))$$
end if

$$x_{\frac{N-i-1}{N}} \leftarrow x_{\frac{N-i}{N}} - \frac{1}{N} f_\theta(x_{\frac{N-i}{N}}, \frac{N-i}{N}, \frac{N-i-1}{N})$$
end for

G Additional Quantitative Results

G.1 Additional Performance

For a detailed comparison among secant losses, we provide more results on CIFAR-10 and ImageNet-256 \times 256 in Table 7.

G.2 Training Efficiency

In practical application, methods like continuous-time CMs [33, 35] and MeanFlow [67] require analytical Jacobian-vector product (JVP) operations to compute the loss. This imposes a significant computational burden, especially in PyTorch. To provide a direct comparison, we benchmark the training speed and memory usage under the same EDM setup (the batch size is 512 on 8 A100 GPUs with 64 per GPU) on CIFAR-10. The results are shown in Table 8.

H Experimental Settings

The detailed experimental configurations are presented in Table 9. Basically, we follow the settings of EDM and SiT. Except for STEE on ImageNet-256 \times 256, we multiply the learning rate by a factor of 0.1. For CIFAR-10 dataset, we use the DDPM++ architecture, and adopts the Trigflow framework. For ImageNet-256 \times 256, we cache the latent codes on disk, and for simplicity we disable the horizontal flip data augmentation. For SDEI, STEI and SDEE, we embed CFG scale as a conditional input to the model, with the CFG range [1, 2] for 2-step, 4-step and 8-step models and [1, 2.5] for 1-step ones. In the experiment concerning training from scratch on ImageNet-256 \times 256,

Table 8: Comparison on training efficiency among different approaches.

Method	Training Speed (sec/KIMG)	Memory Usage (G, Per GPU)
EDM [6] (teacher diffusion model)	0.57	8.69
MeanFlow [67]	1.04	38.73
SDEI	0.91	9.64
STEE	1.42	16.95
SDEE	0.91	9.64
STEI	0.72	9.34

Table 9: Experimental settings of four loss functions on different models and datasets.

	CIFAR-10				ImageNet-256 × 256			
	SDEI	STEI	SDEE	STEE	SDEI	STEI	SDEE	STEE
Model Setting								
Architecture	DDPM++	DDPM++	DDPM++	DDPM++	DiT-XL/2	DiT-XL/2	DiT-XL/2	DiT-XL/2
Params (M)	55	55	55	55	675	675	675	675
σ_d	0.5	0.5	0.5	0.5	-	-	-	-
$c_{\text{noise}}(t)$	$\frac{1}{4} \ln(\sigma_d \tan t)$	t	t	t	t			
Boundary ϵ_1	0.001	0.001	0.001	0.001	-	-	-	-
Boundary ϵ_2	0.00625	0.00625	0.00625	0.00625	-	-	-	-
Initialization	EDM	EDM	EDM	EDM	SiT-XL/2	SiT-XL/2	SiT-XL/2	SiT-XL/2
Training Setting								
Precision	fp32	fp32	fp32	fp32	fp16	fp16	fp16	fp16
Dropout	0	0.2	0	0.2	0	0	0	0
Optimizer	RAdam	RAdam	RAdam	RAdam	AdamW	AdamW	AdamW	AdamW
Optimizer ϵ	1e-8	1e-8	1e-8	1e-8	1e-8	1e-8	1e-8	1e-8
β_1	0.9	0.9	0.9	0.9	0.9	0.9	0.9	0.9
β_2	0.99	0.99	0.99	0.99	0.999	0.999	0.999	0.999
Learning Rate	1e-4	1e-4	1e-4	1e-4	1e-5	1e-5	1e-5	1e-4
Weight Decay	0	0	0	0	0	0	0	0
Batch Size	512	512	512	512	256	256	256	256
Training iters	100K	100k	100k	100k	100K	100k	100k	100k
t, s sampling	discrete	discrete	continuous	continuous	discrete	continuous	continuous	continuous
r sampling	Uniform	Uniform	Uniform	Uniform	Uniform	Uniform	Uniform	Uniform
EMA Rate	EDM's	EDM's	EDM's	EDM's	0.9999	0.9999	0.9999	0.9999
Label Dropout	-	-	-	-	-	0.1	-	0.1
Embed CFG	-	-	-	-	✓	✓	✓	✗
x -flip	✗	✗	✗	✗	✗	✗	✗	✗

we maintain identical settings to those specified in the STEE column, while only disable the pretrained weights and alter the model size. To calculate the FID and IS score at evaluation, we use the codebase provided in MAR [85] for simplicity. The result of Flow-DPM-Solver [79, 16] in Table 3 is with CFG scale of 1.5. All the experiments can be done on a sever with 8 NVIDIA A100 GPUs.

I More Visualizations

Additional visualization results are presented for both datasets. For CIFAR-10 dataset, we provide 4-step and 8-step results using $\mathcal{L}_{\text{SDEI}}$ in Fig. 8 and Fig. 9, respectively. For ImageNet-256 × 256, extended visualizations of 8-step generation using $\mathcal{L}_{\text{STEE}}$ are displayed in Fig. 10 and Fig. 11.

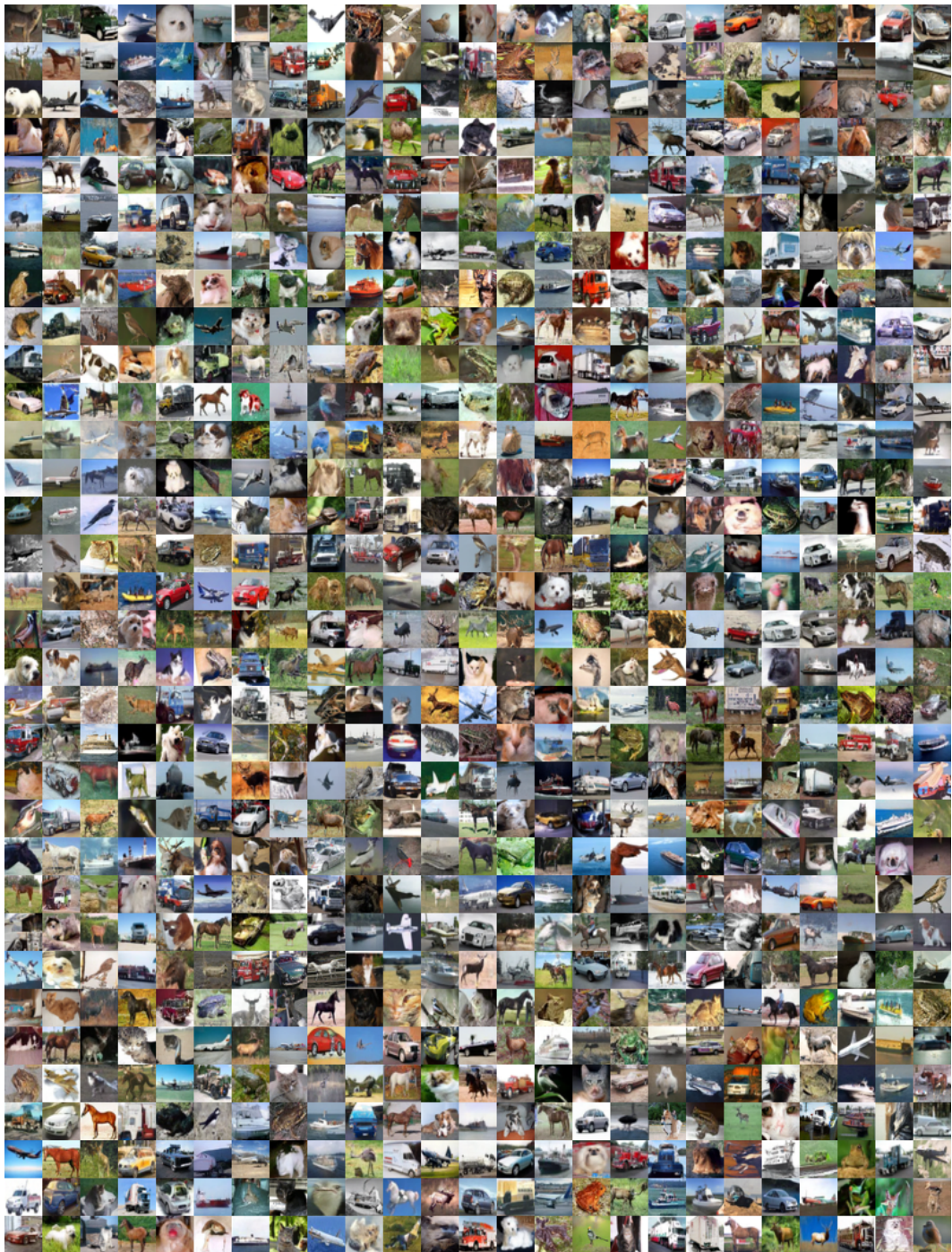


Figure 8: Uncurated 4-step samples on unconditional CIFAR-10.



Figure 9: Uncurated 8-step samples on unconditional CIFAR-10.



Figure 10: Uncurated 8-step samples on ImageNet- 256×256 . Guidance scale is 2.1, and the guidance of first two steps is ignored.



Figure 11: Uncurated 8-step samples on ImageNet- 256×256 . Guidance scale is 2.1, and the guidance of first two steps is ignored.